UNIVERSITY OF CALIFORNIA,
IRVINE

Optimization of Dual Planar Laser Induced Fluorescence (DPLIF) Instrumentation for Characterization of Liquid Mixing in Sprays

THESIS

Submitted in partial satisfaction of the requirements for the degree of

MASTER OF SCIENCE

in Mechanical and Aerospace Engineering

by

Hannah Erin Bower

Thesis Committee:
Professor G. Scott Samuelsen, Chair
Professor Vincent G. McDonell
Professor Derek Dunn-Rankin

2016

DEDICATION

“You can have anything your little heart desires.”

-Grammy Salvadore

TABLE OF CONTENTS

LIST OF FIGURES

LIST OF TABLES

NOMENCLATURE

Greek

Δ	Change
ϵ	Extinction coefficient
φ	Quantum efficiency
h	Planck's constant
v	Frequency
λ	Wavelength
η	Collection efficiency
$g(\omega)$	Appropriate line shape factor
γ	Absorption coefficient
n'	Imaginary part of the index of refraction

Upper Case Roman

P	Power of laser beam
A	Area
C	Constant/Concentration
S_f	Fluorescent Signal
A_{21}	Einstein A coefficient for transition
N_T	Absorber total number density
Q	Electronic quenching rate

Abbreviations

CCD	Charge Coupled Device
DPLIF	Dual Planar Laser Induced Fluorescence
F	Fluorescence
H_2	Hydrogen
ICCD	Intensified Charge Coupled Device
ISO	International Standards Organization
LOX	Liquid Oxygen
LIF	Laser Induced Fluorescence
PLIF	Planar Laser Induced Fluorescence
S2	Excited electronic substate

ACKNOWLEDGEMENTS

I would like to first and foremost acknowledge Professor Scott Samuelsen for providing me with this opportunity to conduct research at UCI and for being my graduate advisor for the past two years. I would also like to acknowledge Dr. Vincent G. McDonell for his assistance, advice and support in my research endeavors. Furthermore, I would like to thank Professor Derek Dunn-Rankin for serving on my thesis committee and for taking the time to assist in the review process.

This project could not have been completed without the help of my fellow lab members, so I would like to extend my acknowledgements to: Scott Leask, Henry Le, Ryan Ehlig, Max Venaas, Fabian Rosner, Jamie Ibrahim, Adam Silver and the rest of the graduate and undergraduate students in the Advanced Power and Energy Program for their friendship and support for the last two years.

ABSTRACT OF THE THESIS

Optimization of Dual Planar Laser Induced Fluorescence (DPLIF) Instrumentation for Characterization of Liquid Mixing in Sprays

By

Hannah Erin Bower

Master of Science in Mechanical and Aerospace Engineering

University of California, Irvine, 2016

Professor G. Scott Samuelsen, Chair

In this effort, a novel Dual Planar Laser Induced Fluorescence (DPLIF) diagnostic is developed and optimized for characterizing the liquid-liquid interactions in rocket injector sprays. A critical attribute associated with the system is a desire to utilize relatively inexpensive components. The newly developed DPLIF diagnostic consists of a camera system, a laser system, and an optics system. The functionality and accuracy of the DPLIF system was determined through stationary liquid and dynamic spray experiments. The results, while preliminary, indicate that the DPLIF system can accurately represent the spatial interactions of two mixing liquids at the same time. Ultimately, the diagnostic shows promise for improved ability to more comprehensively characterize rocket injector sprays and, ultimately, improve rocket injector design.

1 INTRODUCTION

1.1 Overview

Understanding the dynamics of liquid mixing is important in designing and optimizing automotive and aerospace spray systems, such as rocket or automotive fuel injectors. The use of fluorescence, produced by laser-liquid interactions, to better understand liquid structure and dynamics is commonly used as a strategy to isolate the material of interest as elastic laser scattering noise can be suppressed (McDonell, personal communication, May 1, 2016). Fluorescence occurs when a molecule absorbs a photon of a certain wavelength, an electron is excited into a different molecular electronic state and relaxes back down to ground state through the radiation of energy in the form of fluorescence (Skoog et al., 2007).

One of the major applications of fluorescence, with regards to laser diagnostics of sprays, is planar laser-induced fluorescence (PLIF). PLIF is a non-intrusive technique for measuring the concentration in fluid flows (Crimaldi, 2008). The use of fluorescent dyes to visualize the fluid flow was first used in turbulent and laminar flow experiments (Reynolds, 1883). It was then expanded in 1976 through the creation of the laser-induced fluorescence (LIF) technique (Dewey, 1976). LIF was further extended by using a planar laser sheet, producing PLIF, which is the most common two-dimensional LIF technique to study fluid flows today (Crimaldi, 2008).

The extent to which fuel and oxidant are uniformly mixed in combustion systems is of great interest, especially in lean fuel systems where the goal is for combustion at low stoichiometries to ultimately reduce NO_x formation (Kuo, 1996). Furthermore, understanding the

mixing of fuel and oxidant can lead to an increase of combustion efficiency and stability to improve the performance of liquid rocket engines (Jung et al., 2000).

Although PLIF techniques are advantageous in studying fluid flows, commonly used approaches have a fundamental disadvantage, namely two liquids cannot be characterized using fluorescence at the same time. Therefore, it is of interest to explore development of a diagnostic strategy to characterize the mixing of multiple liquids within a spray. This development is the subject of this thesis. The diagnostic method has been dubbed dual wavelength laser-induced fluorescence (DPLIF). Such a diagnostic can ultimately allow for better understanding of the mixing processes of combustion injector sprays such as those found in liquid rocket motors.

1.2 Goal

The goal of this research is to develop, verify, apply and optimize a robust non-intrusive laser-based diagnostic for studying the mixing of two liquids as they interact in a gas phase environment.

1.3 Objectives

The following objectives were established to meet the research goals:

1.) Research, develop and integrate optimized components in an existing DPLIF setup.

2.) Test functionality of individual DPLIF components.

3.) Select applicable experiments to validate DPLIF theory and integrated instrumentation.

4.) Conduct validity experiments using the DPLIF instrumentation.

5.) Analyze data and make relevant conclusions.

The thesis is organized as follows: Chapter 2 provides background and an overview of the theory and previous work in applying LIF to sprays and culminates with open questions this thesis addresses. Chapter 3 describes the approach taken to accomplish the stated goals. Chapter

4 presents the instrument developed and Chapter 5 presents the results of validation experiments. Finally, Chapter 6 presents conclusions and suggestions for future work are discussed.

2 BACKGROUND

Liquid-liquid mixing occurs in many applications. In polymer processing, mixing greatly affects the material properties, cost and processability. Reinforcing materials and additives are mixed with polymers to improve flame or corrosive retardance and increase impact toughness. However, it is impossible to accurately predict how efficiently a particular processor will mix from a theoretical basis (Rauwendaal, 1991). Therefore, a better understanding of the mixing process in polymer solutions is needed to better design polymer processing equipment. Furthermore, in chemistry, fluid mixing can lead to organic synthesis. For example, aqueous fluids with differing compositions are usually far from thermodynamic equilibrium when they mix, thus providing a source of free energy that can drive organic synthesis (Shock et al., 1998). Since hydrothermal circulation can lead to fluid mixing on any planet with liquid water and a source of heat, understanding the mixing of liquids, could give a better understanding of whether the creation of organic compounds on another planet is possible.

Although many applications in science and engineering require better understanding of mixing liquids, combustion is a field of study where the mixing of oxidant and fuel directly relates to the performance of the system. For example, liquid rocket injector sprays is a subfield in need of further research in mixing analysis. Rocket engine design and performance significantly depends on the liquid fuel's ability to atomize and mix appropriately with liquid oxidant. Many types of injectors can be used for different space propulsion applications. For example, pintle injectors have been used on second stage engines, such as the Delta Engine (Dressler, 2000), unlike doublet injectors have been used on the Apollo service module (Hefner, 1966), and coaxial injectors have been studied and used extensively in NASA's Liquid Rocket Engine (LRE) combustors (Kenny et al., 2006). Through better understanding of the mixing

processes of these injectors, improved, more optimal injectors that produce a more evenly distributed, homogenously mixed sprays can be designed. This need motivates the development of the DPLIF diagnostic which is the subject of this thesis.

2.1 Laser Diagnostics

With the increasing availability and reliability of optomechanical devices and sensors, laser spectroscopy has become a commonly used technique for studying combustion processes. Laser diagnostics allow for in-situ, precise and nonintrusive measurements and have advantages over manual probing methods. For example, laser techniques are nonintrusive and therefore will not alter the spray or flame behavior, providing more accurate results. Also, laser diagnostics allow for in-situ measurements, removing the need for corrections to errors present when physical probes or large spectrometers are used. Furthermore, a main advantage to using lasers is that they can reach high light intensity powers, which allows for before unnoticeable processes to be analyzed (Eckbreth, 1996). The laser light provides enough energy to the spray to allow fluorescent molecules to be excited and emit fluorescence that is captured by a camera. This enables the LIF technique to be used to characterize high velocity, small diameter spray droplets. Without powerful reliable lasers and associated sensors, both PLIF and the novel DPLIF techniques would not be possible.

2.2 Fluorescence

Fluorescence is a widely used diagnostic tool. The fluorescence process is a part of the luminescence family, where molecules emit light as they relax from electronically excited states. The excitation of molecules by ultraviolet or visible light photons, photoluminescence, can be divided into fluorescence and phosphorescence depending on the electron relaxation pathway (Herman et al., 2009). Figure 1, is the Jablonski diagram, which depicts the process for both fluorescence and phosphorescence (Wong, 2014). In fluorescence, a fluorescent molecule (e.g.,

oxazine, fluorescein) absorbs a specific wavelength photon, exciting an electron in the fluorescent molecule to an excited electronic substate (S2). The electron then undergoes internal conversion, the passing to a lower energy electronic state without emission of radiation, where it then emits radiation (fluorescence) to get back to ground state (Skoog, 2007).

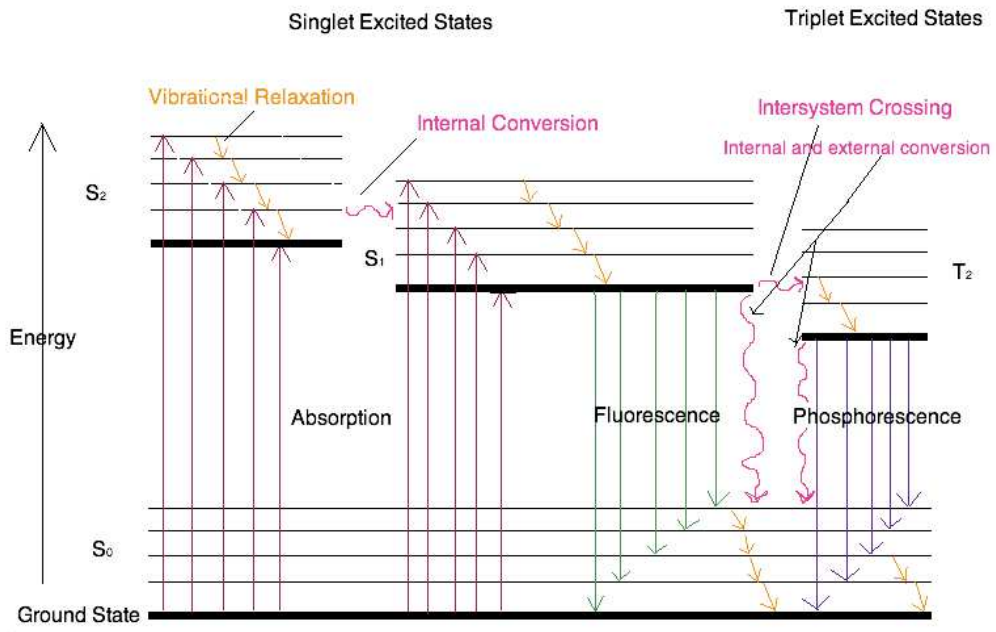

Figure 1. Jablonski diagram of fluorescence and phosphorescence (Skoog, 2007)

The use of fluorescence with photographic methods can be a sufficient technique to further understand macromixing processes occurring in combustion injector sprays. Fluorescence is a nonintrusive, in-situ technique used to determine local concentrations of fuel and oxidizer captured by a light sensitive camera. Fluorescence theory, using fluorescent molecules and intensified laser light, allows for the development of PLIF and DPLIF techniques. Without fluorescence, the DPLIF technique would not be useful in characterizing the liquid fuel and oxidizer interactions within the combustion chamber.

2.3 Laser Induced Fluorescence (LIF)

The combination of intensified laser light and fluorescent molecules leads to LIF and PLIF techniques. LIF can be used to measure liquid-liquid interactions at a point, line and in two dimensional planes. To assess the mixing and dispersion of liquid-liquid interactions, the fluorescent signal produced and captured by the camera needs to be analyzed. The PLIF fluorescent signal is based off the theory where the relationship between fluorescent intensity and the liquid mass is dependent on the characteristics of incident light, the photophysics of the fluorescing media and the characteristics of the imaging optics (McDonell, Samuelsen, 1997). According to Kychakoff et al. (1982), the fluorescence signal (S_F) in the plane illuminated by the laser depends on the incident photons, absorbed photons, fluorescence quantum yield and collection efficiency, as displayed below in Equation 1.

$$S_f = \frac{E}{hv} n\sigma(\lambda, T)\phi(\lambda, T, p_i)\eta \qquad \textbf{Equation 1}$$

In Kychakoff's equation, $\frac{E}{hv}$ represents the incident photons, $n\sigma(\lambda, T)$are the photons absorbed, (λ, T, p_i) depicts the fluorescence quantum yield and η is the collection efficiency.

$$S_f = \frac{E}{hv} n\sigma(\lambda, T)\phi(\lambda, T, p_i)\eta \qquad \textbf{Equation 1}$$

Based on

$$S_f = \frac{E}{hv} n\sigma(\lambda, T)\phi(\lambda, T, p_i)\eta \qquad \textbf{Equation 1}$$

, it is clear that laser intensity and the absorber total number density have a direct effect on the fluorescence signal captured by the camera. Therefore, the laser power and concentration of the fluorescent are directly proportional to the fluorescent signal produced by the liquids of interest.

In 1989, Sreenivasan and Prasad demonstrated the use of LIF for point measurements, while in 1985, Koochesfahani and Dimotakis determined concentrations along a line. Additionally, Dahm and Dimotakis (1987) demonstrated the use of LIF along a plane. Dahm and Dimotakis' experiments used a collimated 514.5nm laser beam from a 10W argon laser arranged to form a single thin sheet containing the jet axis or a pair of mutual orthogonal sheets intersecting on the jet axis. Dahm and Dimotakis used the LIF technique to determine the axial distance required to molecularly mix every part of the jet fluid with ambient fluid to the stoichiometric value.

Furthermore, Komori et al. (1993) demonstrated the use of LIF techniques to measure scalar concentrations at a point and Papantoniou and List (1989) measured scalar concentrations along a line. Dahm and Dimotakis (1987) also demonstrated the use of LIF techniques to acquire two-dimensional planar measurements and LIF was further enhanced when Van Vliet et al. (2004) measured scalar concentrations in three-dimensional planes.

Recent advances have been made to produce more commercialized, compact LIF instrumentation. Dantec, TSI and La Vision have developed "turn-key", easy to use, LIF and PLIF systems. However, commercialized LIF systems are not cost-effective, at retail prices over $150,000. Additionally, Fang et al. (2016) recently developed a handheld LIF detector for multiple applications. The handheld LIF detector uses a 450nm laser diode, which is passed through a 2.0mm aperture, a 450nm band-pass filter and then reflected by a dichroic mirror and focused by a collimating lens. The emitted fluorescent light is then collected by the same collimating lens, passed through the same dichroic mirror and band-pass filter, reflected by a mirror and passed through a 1.0mm aperture. Finally, the fluorescence beam is detected by a

miniaturized photomultiplier tube and an output signal is acquired by an electric circuit and displayed on the screen of the detector. The LIF schematic is displayed below in Figure 2.

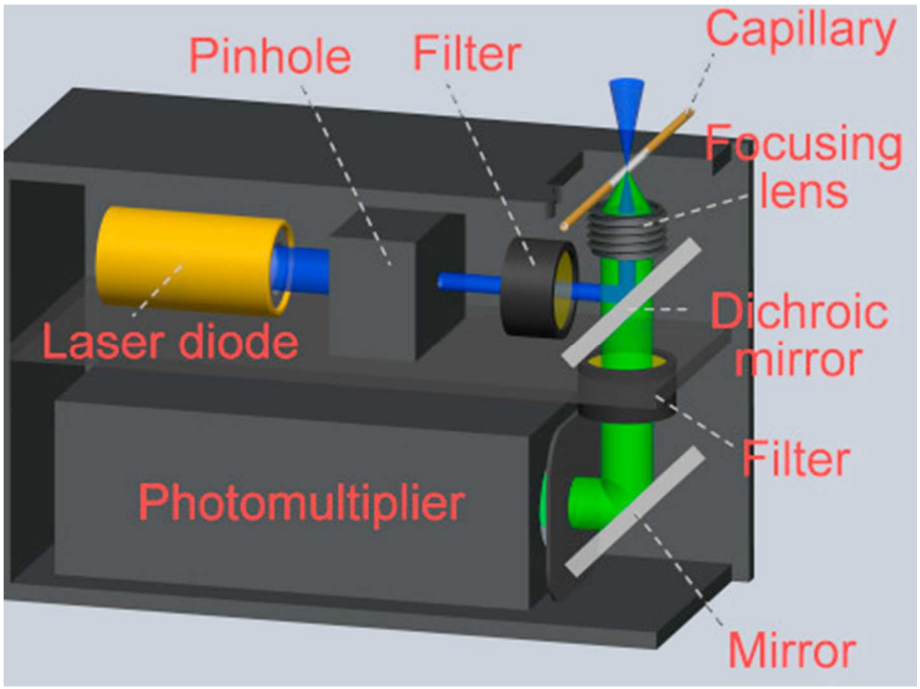

Figure 2. Handheld LIF detector Schematic (Fang et al., 2016)

In addition, Melton (1993) created an exciplex variation to the LIF theme which allowed for spectrally separated fluorescence from the liquid and vapor phases (Fansler, 2015). This technique adds two organic tracer species to non-fluorescing liquid. An ultra-violet laser then excites one of the fluorescent tracers (excited monomer), which emits fluorescence in the gas phase. In the liquid phase, the excited monomer can combine with the other fluorescent tracer in its ground state to form an excited complex (exciplex). Fluorescence from the exciplex is red-shifted due to the binding energy of the complex and therefore, can be distinguished from the excited monomer's fluorescence (Fansler, 2015). Consequently, the exciplex technique allows for the differentiation of the fluorescence of species in the gas and liquid phases.

The most common application of the LIF technique in studying liquid-liquid interactions is through the use of a two dimensional planar sheet, PLIF. Figure 3 displays the basic schematic of the PLIF setup (Crimaldi, 2008). PLIF uses a series of focusing, cylindrical and planar lenses to create a uniform planar laser sheet. The two-dimensional planar sheet allows for more conclusive images and conclusions of the local and overall mixing of the two liquids.

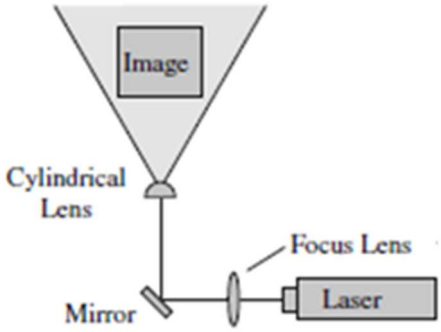

Figure 3. Basic PLIF Schematic (Crimaldi, 2008)

Van Vliet et al. (2004) used PLIF for determining liquid-liquid concentrations in three dimensional volumes. Figure 4 displays the Van Vliet et al. PLIF system. Van Vliet et al. used a 488nm continuous laser that was widened into a horizontal sheet by a negative cylindrical lens. The sheet was then swept in the normal direction by a low-inertial Galvano mirror. Using a high speed CCD camera to capture the fluorescence of the sweeping sheet, three dimensional concentrations were measured.

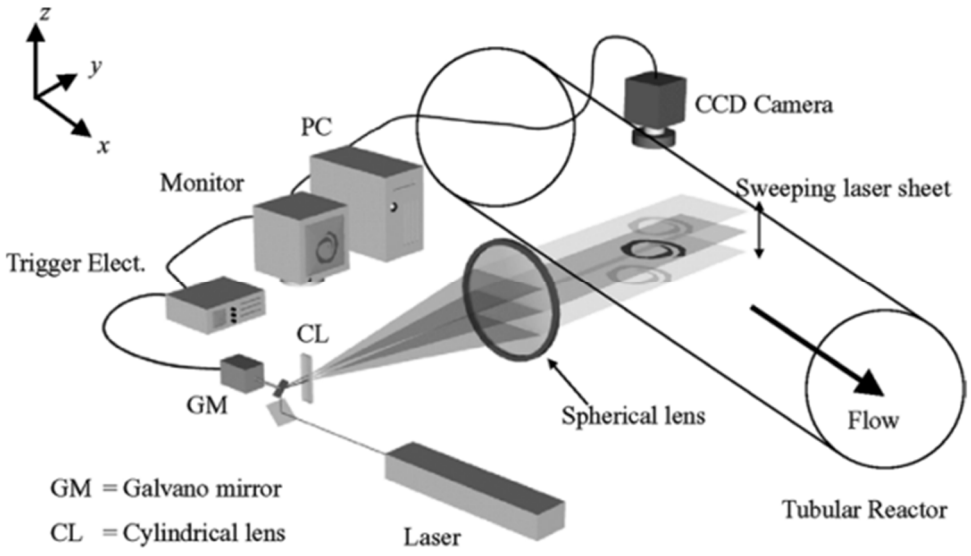

Figure 4. Three dimensional measurement PLIF schematic (Van Vliet et al., 2004)

McDonell et al. (1999) tested the PLIF concept in unlike doublet injector spray studies to assess the mixing and dispersion of oxidizer and fuel liquids. By dying the oxidizer and fuel selectively with different fluorescents, exciting the dyes with optimal wavelengths and using a selection of filters to isolate one or the other, the mixing effectiveness of two fluids could be evaluated. But the two liquids could not be measured simultaneously which necessitated a highly repeatable experiment and duplication of run conditions which are time consuming and not always practical.

Furthermore, Lockett et al. (2016) used PLIF along with Mie scattering to acquire data in a Laser Sheet Dropsizing (LSD) experiment on the atomization of non-evaporating diesel sprays. The LSD experiment required simultaneous high speed imaging of planar laser Mie scattering and PLIF. Hence two wavelengths are involved, but each is used for a different characteristic of the spray (fluorescence and scattering). A 527nm pulsed laser passed through a 50mm diameter focusing lens and an 8x cylindrical telescope to form a laser sheet 20mm high and 0.25mm

wide. The laser sheet was passed through the center of the spray emitted from the nozzle, producing elastic Mie scattering at 527nm and broad-band Rhodamine-B PLIF scattering between 570-590nm, which was captured on a Photron FASTCAM SA1.1 high speed video camera (Lockett et al., 2016).

Despite the advantages of PLIF, one main disadvantage is that the commonly used setups do not allow for fluorescing two liquids at the same time, thus adding experimental errors when analyzing the liquid-liquid mixing interactions between the two fluoresced liquids. The combined fluorescence/scattering methods provide an example of the basic approach on the light source side, but the interpretation of the two signals is different. Although it is possible that the liquid interactions are stable throughout data collection, this is not always the case. Thus, inaccuracies of local fluorescent concentration could occur, creating error in the liquid-liquid interactions analysis. Therefore, this thesis presents the DPLIF technique that would ultimately reduce experimental errors by enabling fluorescence and data acquisition of both liquids simultaneously.

2.4 Dual Planar Laser Induced Fluorescence (DPLIF)

The DPLIF technique utilizes similar theory and instrumentation to the PLIF technique. Like PLIF, DPLIF is expected to produce at least semi-quantitative results. The ability to record and analyze the fluorescence signal of two different fluorescents at the same time is a major difference and advantage to DPLIF over the commonly used PLIF technique. Melton's exciplex variation on the LIF technique demonstrated the use of fluorescing two organic tracers simultaneously (Fansler, 2015). However, only one laser was used to excite the tracers and the exciton technique is utilized to understand vaporizing sprays not liquid-liquid interactions. Additionally, Le Gal, Farrugia and Greenhalgh (1999) performed laser sheet dropsizing of dense

sprays experiments that utilized the idea of collecting fluorescence data and Mie scattering data at the same time. Although Le Gal et al. did not use PLIF with two different liquids, their experiments employed the idea of using either two CCD cameras to obtain both data sets, or by imaging the spray onto two halves of the same CCD array using a combination of mirrors, beamsplitters and filters (Le Gal et al., 1999).

A major consideration that needs to be taken into account when using DPLIF is whether one wavelength affects the results of the other and vice versa. This effect has direct implications for wavelength selection and dye selection which in turn impacts the signal isolation on the detector side. Ideally the two exciting wavelengths will be as close as possible to minimize this effect, but the closer they are together, the more difficult it is to optically isolate the fluorescence signals. This concern can be addressed through evaluating the scattering efficiencies of both the wavelengths used in the DPLIF system. At an absorbing wavelength, the extinction I/I_0 can be broken down into drop scattering, drop absorption and vapor absorption components, as indicated in the equation

$$\frac{I}{I_0} = \exp\left[-\overline{C_n} l \frac{\pi}{4} \int_0^\infty Q_{ext} D^2 \overline{N(D)}\, dD\right] * exp\left[-\overline{C_n} l \frac{\pi}{4} \int_0^\infty Q_{abs} D^2 \overline{N(D)}\, dD\right] * \exp(-k_v \overline{P_v} l) \qquad \textbf{Equation 2}$$

Where $\overline{C_n}$ is the average number density of the drops, l is the average path length, $\overline{N(D)}$ is the drop diameter distribution, k_v is the absorption coefficient of the liquid studied and $\overline{P_v}$ is

the average liquid concentration (Drallmeier, 1994). The scattering efficiencies of each laser can be determined using

Equation

$$I/0=\exp-Cnl\pi 40\infty\ QextD2NDdD*exp-Cnl\pi 40\infty\ QabsD2NDdD*\exp\ (-kvPvl)$$

Equation 2

$$Q_{ext} = Q_{sca} + Q_{abs}$$ **Equation 3**

Where Q_{ext} describes the drop extinction characteristics and Q_{sca} and Q_{abs} are the scattering and absorption efficiencies, respectively (Drallmeier, 1994). The scattering efficiency is derived from the integration of the scattered power in all directions and the extinction efficiency is derived from the Extinction Theorem (Maetzler, 2002; Van De Hulst, 1981). From determination of the scattering efficiencies of the two lasers used in DPLIF, it can be determined if a correction factor is needed to account for differences in scattering efficiency when using different wavelength lasers.

In previous DPLIF experiments, a series of lenses were used to match the focus and divergence of both wavelengths (in this case 447nm and 655nm), to ensure beam intensity and correct for beam differences. Figure 5 displays the DPLIF setup used by Bolszo (2011). A five watt Argon-Ion laser (Coherent model Innova I-90C) in multi-line mode and a 1.5 watt 655 nm double pumped solid-state laser (OEM Laser Systems, Inc. model PSU-III LED) were used in

Bolszo's setup. An intensified CCD camera (Princeton Instruments model 375-E) with Micro Max intensifier and WinView/32 (version 2.5.21.0) analysis software were used to capture time averaged images and geometric optics were used to match the beam shapes and divergence. A dichroic mirror and negative concave lens were used to diverge the laser beams into a planar sheet (Bolszo, 2011). A similar DPLIF setup was used in Sung's (2014) experiments to study the effects of water-in-oil emulsions on diesel fuel combustion performance.

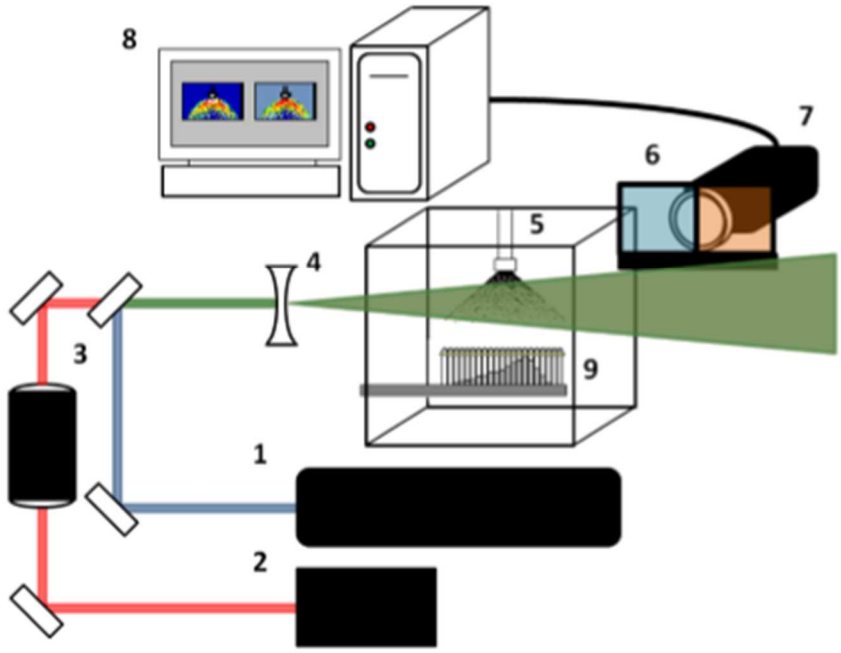

Figure 5. DPLIF original setup: 1) Argon-Ion laser, 2) red diode laser, 3) geometric optics setup to match beam shape into dichroic mirror, 4) diverging lens, 5) emulsion spray test section, 6) optical filters, 7) high intensity CCD camera, 8) PC with intensifier and analysis software, and 9) mechanical spray half-patternator. (Bolszo, 2011)

Although the original DPLIF setup functioned, some weaknesses exist in the system. The original setup required careful positioning of lenses to allow for optimal alignment into a sheet. If one lens was slightly unaligned, the plane shape, intensity and uniformity would be affected.

This led to constant instrumental errors and inconsistent data. Also, the original setup occupied $1m^2$ of space, which is not ideal for a commercialized system. Therefore, a series of improvements were made to increase the planar reliability of the DPLIF system and to decrease the size of the overall system.

2.5 Applications for DPLIF in Liquid Rocket Injectors/Combustion

PLIF and DPLIF techniques can be useful for understanding the liquid-liquid interactions, especially concentration and mixing, of many different types of aerospace injectors. Three injectors commonly used in rocket engines that could benefit from more spray characterization studies using the DPLIF technique are pintle injectors, unlike doublet injectors and coaxial shear injectors.

2.5.1 Pintle Injectors

The Pintle injector is one of the most reliable, cost effective and efficient injectors used for rocket propulsion. The pintle injector, displayed in Figure 6 (Dressler, 2000; Dong, 2013), has been used in various types of rocket engines, such as the lunar module descent engine (LDME) (Dressler and Bauer, 2000) and is currently being used in the development of the SpaceX Falcon 9 rocket's Merlin engines ("SpaceX: Falcon9", 2014). The success of the pintle injector lies within its design. The injector generally consists of a post with multiple holes/slots at the tip. The fuel flows down the center of the post and radially out through the holes, while the oxidizer flows in a thin annular sheet along the surface of the post (Heister, 2011). The collision of the fuel and oxidizer creates a curved spray that is considerably different from the spray created by early "flat face-type" injectors (Heister, 2011). Due to the simplicity of the pintle design, a pintle engine is simpler to build, has higher combustion stability and higher throttle ability than other types of injectors.

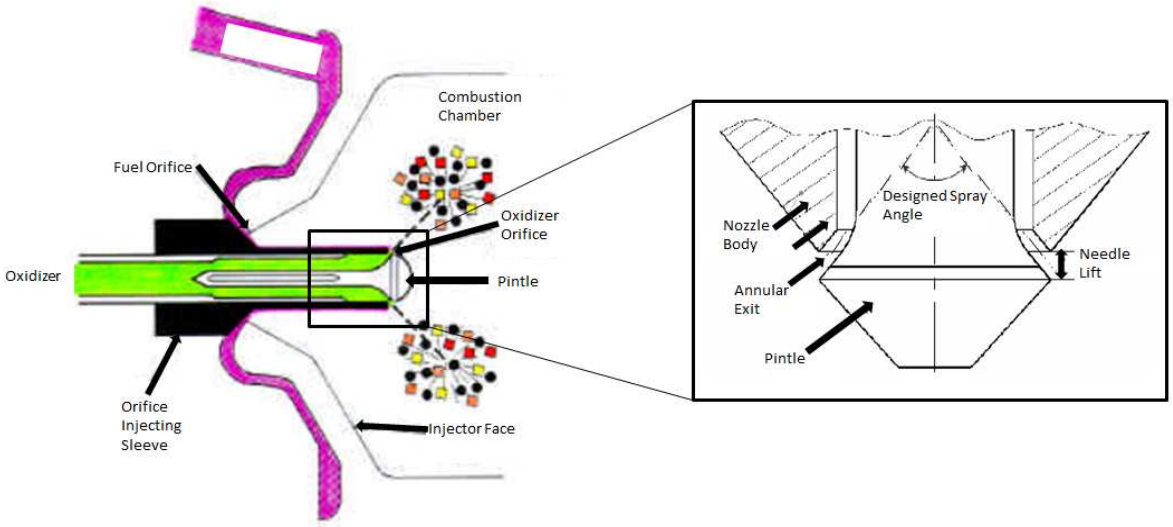

Figure 6. Pintle injector schematic (Heister, 2011)

Experiments aimed at understanding the cold flow (i.e., atomization, dispersion, and mixing evaporation) behavior of aviation and rocket fuel using pintle injectors have not been sufficiently studied to date. S.D. Heister proclaims in the *Handbook of Atomization and Sprays* (2011) that pintle injector flow characteristics are less studied than flat faced injectors. According to Heister, information regarding droplet sizes of various pintle injector designs is not yet sufficiently available in literature. Most tests on pintle injector engines, such as the Lunar Module Decent Engine (LMDE) and the SENTRY Pinch and Yew engine consist of only hot-fire tests, as mentioned in the "TRW Pintle Heritage and Performance Characteristics" paper by G.A. Dressler (2000). In a study performed by B.L. Austin and S.D. Heister (2005), the characterization of pintle engine performance for nontoxic hypergolic bipropellants were determined through only hot-fire testing. Additionally, T. Mueller and G. Dressler (2000) studied the engine test results of a 40KLBf LOX/RP-1 low cost pintle engine, where combustion efficiency, thrust and total work were determined for varying pintle configurations. However, few hot-fire tests have been coupled with cold-flow tests. Therefore, further studies in the cold-flow characteristics of pintle sprays, such as fuel and oxidant mixing characterization tests, could

lead to more efficient and stable rocket propulsion systems. Furthermore, mixing characterization tests may be more time and cost effective diagnostic tests than hot-fire testing. In order to comprehensively understand the cold-flow and mixing behavior of pintle injectors, better laser diagnostic techniques need to be developed.

2.5.2 Unlike Doublet Injectors

Unlike doublet injectors are one of the most common liquid rocket propulsion injectors. Unlike doublet injectors, displayed in Figure 7, contain a simple manifold and provide good overall mixing and atomization for high performance (Purdue University, 2007). This injection type is best for propellants with equal or nearly equal momentum ratios and fuel/oxidizer injection orifice areas (Ito, 2004). Unlike doublet injectors have most commonly been used for the LEM ascent engine, the Delta launch vehicle and almost all high response attitude control engines that use storable propellants (Purdue University, 2007).

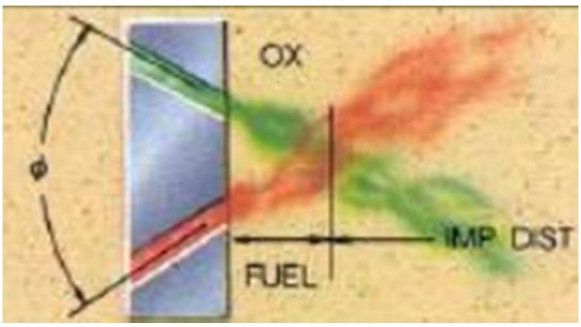

Figure 7. Unlike doublet injector schematic (Heister, 2011; Dong et al., 2013)

Aspects of the atomization characteristics of impinging jets have been thoroughly examined. For instance, H. M. Ryan et al. (1995) determined the sheet breakup length, distance between adjacent waves and drop-size distributions of impinging jet sheets. The observation of flow patterns generated by unlike doublet injectors has also been studied sufficiently, especially through the experiments performed by W.H Lai and H.C. Wang (Lai et al., 2002). As a result of

extensive tests, it was found that unlike doublet injectors tend to produce finer atomization than like doublet injectors, usually have higher performance, but are less stable (Ito, 2004).

While certain characteristics of unlike doublet injector sprays have been sufficiently studied, there are only a few studies on the macromixing processes and the mechanisms involved in the mixing processes of the two liquid streams are available (Ashgriz et al., 2001). One study by Ashgriz et al. (1995) revealed that different processes in the pre-atomization and post-atomization regions control mixing. The study found that turbulent fluctuations and aerodynamically generated helical disturbances on the jet surface downstream of the orifice govern the mixing process in the pre-atomization region and turbulent dispersion in the post-atomization region improves mixing (Ashgriz et al., 1995). Although this study tried to further understand the mechanism of mixing in doublet injector sprays, available literature is mainly concerned with the development of correlations for the spatial distribution of two components of impinging jets spray and the physical configuration of the injection system, thus very little information exists regarding the mechanism of the mixing between the impinging streams (Ashgriz et al. 1995).

Furthermore, the performance of rocket engines is closely coupled to the mixing of the biliquid propellant streams (Ashgriz et al. 1995). Therefore, further understanding the mixing processes of these injectors is vital to optimizing the performance of rocket engines. Through studying unlike doublet injector sprays using the DPLIF technique, it is possible to determine mixing rates of the fuel and oxidizer that can be correlated to combustion performance, which ultimately aids the creation of more stable, higher performing rocket engines.

2.5.3 Coaxial Shear Injectors

Coaxial shear injectors (concentric tube) are commonly used in cryogenic-propellant engines (Vingert et al., 2004). Coaxial shear injectors are known for high performance and stability with LOX/H_2 as the oxidant/fuel (Purdue University, 2007). Coaxial shear injectors, displayed in Figure 8 (Purdue University, 2007; Lepore 1991), have been used in the space shuttle main engines and preburners, in J-2 rockets and orbit transfer vehicles (Purdue University, 2007).

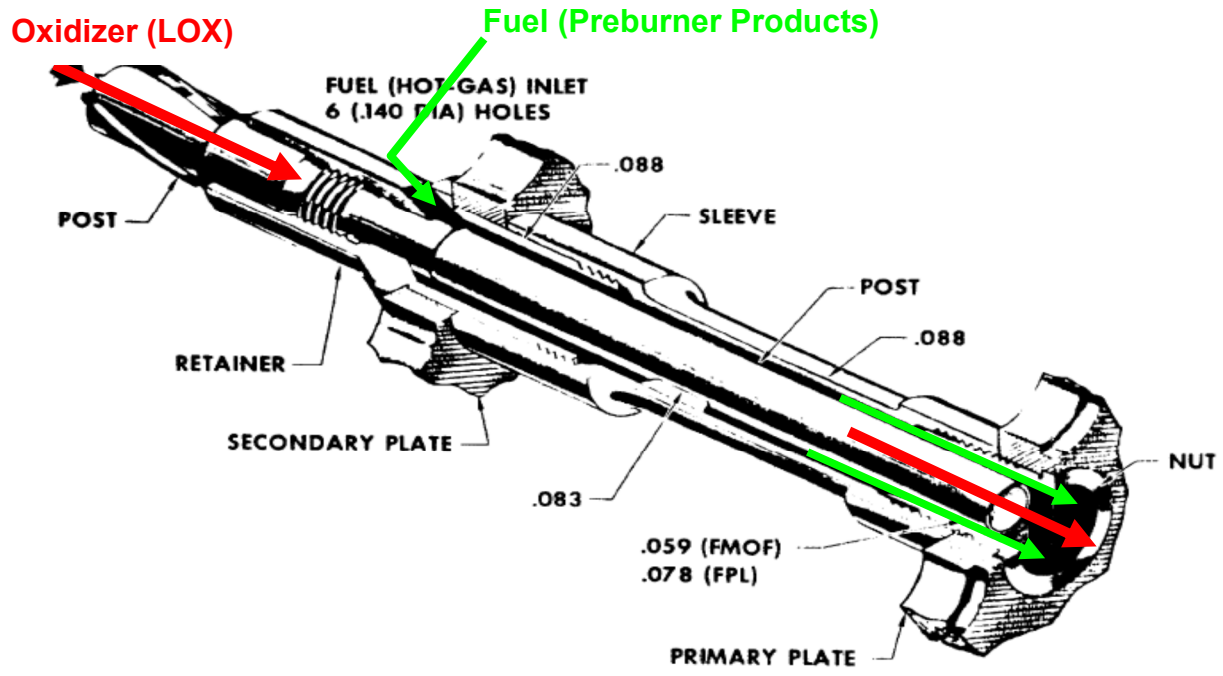

Figure 8. Coaxial shear injector schematic (Purdue University, 2007; Lepore 1991)

In a coaxial shear injector, the liquid sheet breakup and atomization occurs by coflowing high-velocity gas stream with the injector liquid stream (Vingert et al., 2004). In the atomization process, the difference in velocity between the gas jets and liquid jet close to the nozzle leads to surface instability, which leads to primary atomization. Farther from the nozzle, the gas velocity

decreases, leading to secondary atomization (Vingert et al., 2004). Strakey et al. (2001) studied the spray of shear coaxial injectors using strobe backlight imaging, laser sheet spray imaging, mechanical patternation and phase Doppler interferometry. Furthermore, Salgues et al. (2006) performed experiments to help better understand the spray structure, atomization and mixing processes of coaxial shear injector spray through OH PLIF and OH chemiluminessence techniques.

Through studies present in the literature, it is clear that laser diagnostics and PLIF techniques are used in understanding shear coaxial injectors. However, very few PLIF experiments have been performed on coaxial shear injectors to understand the mixing of fuel and oxidant before the combustion processes occur. Using the PLIF technique to study the mixing of the spray instead of the flame is a more time and cost effective method for studying the stability and efficiency of coaxial shear injectors. Therefore, further enhancement of the PLIF technique and the creation of the DPLIF technique could lead to more dependable, improved shear coaxial injector spray characterization conclusions.

2.6 Summary of Background

From this review of laser induced fluorescence injector spray diagnostics in literature, it is clear a need exists for further understanding mixing processes of rocket injector sprays, including pintle, unlike doublet and coaxial shear injectors. While laser diagnostics for understanding mixing exist, weaknesses in existing techniques, such as high cost and system complexity, exist, therefore, use of a DPLIF system can lead to better designed and performing rocket injectors. From here, there are still a number of questions to address in the development of the DPLIF system:

1. The original DPLIF system, created by Bolszo in 2011, used a series of lenses to focus the two lasers together into a single sheet, but is there a more optimal, space efficient way to combine the lasers? Thus it would be beneficial to look into other techniques to combine two laser beams.
2. Would the use of two different lasers together cause interference in the results? If interferences occur, the data could be skewed and the results not reliable. Therefore, tests to further understand the scattering efficiency of the two wavelength laser beams used and the properties of the fluorescent molecules used would be helpful in eliminating potential errors in the setup and technique.
3. Currently, a $40,000 ICCD camera is used to take PLIF/DPLIF measurements. However, when one camera is used by itself, both liquids cannot be examined at the same time, without the use of a $10,000 image splitter, causing an uncertainty in the results. Would it be possible to use two less expensive cameras to capture the fluorescence of the fuel and oxidizer in the spray? Therefore, it would be beneficial to research and test different camera techniques to capture the fluorescence of both liquids at the same time.
4. The DPLIF was originally thought to be used for better understanding the spray characteristics of the oxidizer and fuel of rocket injectors. However, the DPLIF could potentially be used for many different liquid-liquid mixing applications. Thus, it is beneficial to test the DPLIF proof of concept for different mixing applications and setups.

To address these issues, an experimental effort will be conducted to provide a systematic optimization and proof of concept of the DPLIF instrumentation and theory. This will involve design, development and experimentation of all major components of the DPLIF system along with system testing for different applications. This effort will conclude with recommendations on

how to further optimize the DPLIF and how this instrumentation would be most useful with regards to laser diagnostics.

3 APPROACH

The goals of this research are to develop and apply a robust non-intrusive methodology for assessing mixing of two liquids as they interact in a gas phase environment. The tasks described below outline the steps that will be taken to carry out the research goals.

Task 1: Research, develop and integrate optimized components in an existing DPLIF setup

Given the existing DPLIF setup, it will be important to identify the components of the system that can be changed and optimized. One of the main goals in DPLIF system optimization is to create a more compact, cost effective setup. Testing different cameras, fluorescent dye choice and optical setups will allow for the most optimal system to be constructed.

Task 2: Test functionality of individual DPLIF components

The functionality and performance of each optimized component in the DPLIF system will be tested and analyzed. Components include: fluorescents, cameras, optical setup and image registration code. Image analysis software, such as Matlab, ImagePro and ImageJ will be used to determine the performance of the fluorescent compounds and the camera setup. Redesign and testing will occur until each component is functioning sufficiently and deemed optimal.

Task 3: Select applicable experiments to validate DPLIF theory and integrated instrumentation

Primarily, proof of concept tests will be conducted to validate the DPLIF theory and instrumentation. First, the determination of whether one wavelength affects the results of the other and vice versa needs to be concluded. Therefore, the differences in scattering efficiency of the two lasers will be determined. Next, cuvette experiments with 100% oxazine solution, 50%

oxazine-50% fluorescein solution and 100% fluorescein solution will be performed to determine whether the DPLIF system produces similar fluorescent results as to what is expected. Finally, spray experiments will be performed to determine the DPLIF system's ability to analyze the mixing of liquid-liquid interactions in sprays.

Task 4: Conduct validity experiments using the DPLIF instrumentation

The proof of concept experiments will be conducted mainly using the DPLIF system. The scattering efficiency experiments will be conducted using the diode lasers that make up the DPLIF system and a UV-Vis spectrometer. The selected fluorescent dyes will be tested concurrently with the selected cameras to ensure functionality for sprays. The cuvette experiments will implement cuvettes of mixtures with known concentrations of oxazine and fluorescein into the DPLIF system for analysis. The spray experiments will utilize a simplex nozzle and unlike doublet injectors to mix the fluorescein (fuel) and oxazine (oxidizer) fluids for the DPLIF system analysis.

Task 5: Analyze data and make relevant conclusions

A Matlab code along with ImageJ and ImagePro software will be used to analyze the images produced by the camera system. This will involve techniques such as line intensity profiles, area intensity calculations and image fluorescent intensity comparisons. Finally, the images will be processed and the DPLIF instrumentation validity will be assessed.

4 RESULTS AND DISCUSSION

The original DPLIF system contained some weaknesses, therefore, a series of improvements were made to increase the planar reliability of the DPLIF system and to decrease the size of the overall system. This chapter discusses the DPLIF system optimization techniques and results as well as DPLIF instrumentation application test results.

4.1 DPLIF Optimization

The DPLIF instrumentation is comprised of three component systems: the laser system, the optics system and the camera system. Figure 9 displays a block diagram of the DPLIF instrumentation systems and components within each subsystem that were enhanced. In the Lasers System, the fluorescent choice and scattering efficiency dependence on wavelength were two components analyzed and optimized. In the Optics System, optomechanical enhancements were performed. Furthermore, in the Camera System, the camera selection and the image registration code were two components further enhanced. The block diagram also contains a "sample" component, which was composed of an unlike doublet injectors test stand, displayed in Figure 10. The magenta plane depicted in the test stand image is the fluorescent plane and the red "horseshoe" is the fluoresced spray structure. The unlike doublet injectors test stand was used for the various DPLIF component optimization tests.

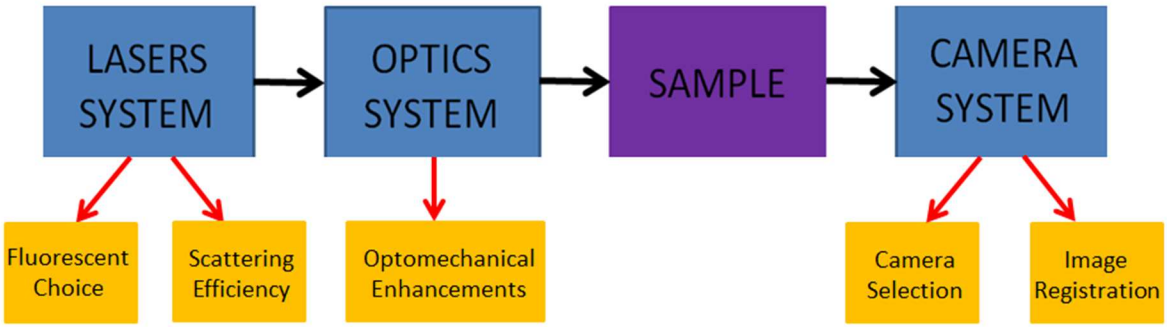

Figure 9. DPLIF instrumentation and enhanced components block diagram

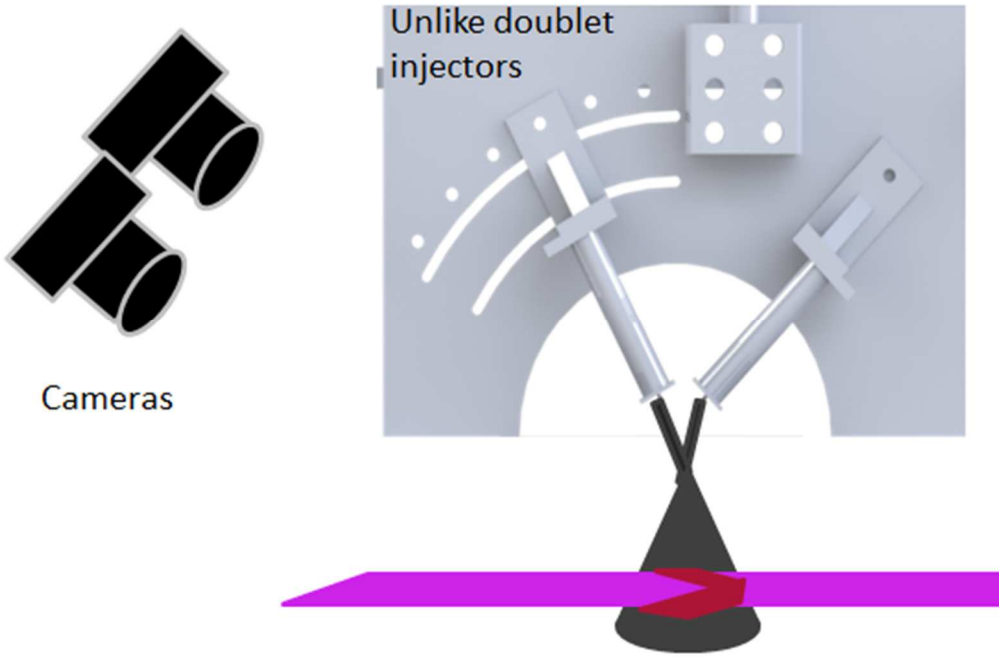

Figure 10. Unlike doublet injectors test stand schematic

4.1.1 Fluorescent Choice

A set of requirements were defined when trying to determine appropriate fluorescents to use, as displayed in Table 1. For example, fluorescein and oxazine were chosen because they were thought to fluoresce well when excited at 447nm and 655nm, respectively, and they would be able to produce fluorescence in the visible spectrum to avoid having to use expensive ICCD or NIR type cameras. Also, they are soluble in water, which was the solvent used for both the "fuel" and "oxidizer" throughout the tests performed in this thesis. Fluorescein perchlorate and Oxazine725 were the fluorescents chosen and used with the original DPLIF system. However, both originally used fluorescein and oxazine derivatives were ultimately determined to be inadequate for the remainder of the experiments.

Table 1. Fluorescent choice requirements

Requirement
High absorbance at 447nm/655nm

Fluorescence in visible spectrum
Solubility in water
High quantum yield

Fluorescein perchlorate has an optimal excitation wavelength at 499nm, however throughout the experiments fluorescein was excited by a 447nm diode laser. Although the 447nm laser is only 52nm different from the optimal excitation wavelength, when the 447nm laser excites the Fluorescein perchlorate molecules, only a 20% relative intensity compared to that of fluorescein at 499nm is produced, as shown in Figure 11 ("Life Technologies Fluorescence SpectraViewer", n.d.). The decrease in relative intensity was apparent in optimization experiments. In preliminary experiments, the fluorescein excited by the 447nm laser could not be detected by the Andor iStar ICCD camera at any mass flow rates tested. Therefore, it was considered best to use a fluorescent that produced higher relative intensity when using the 447nm laser.

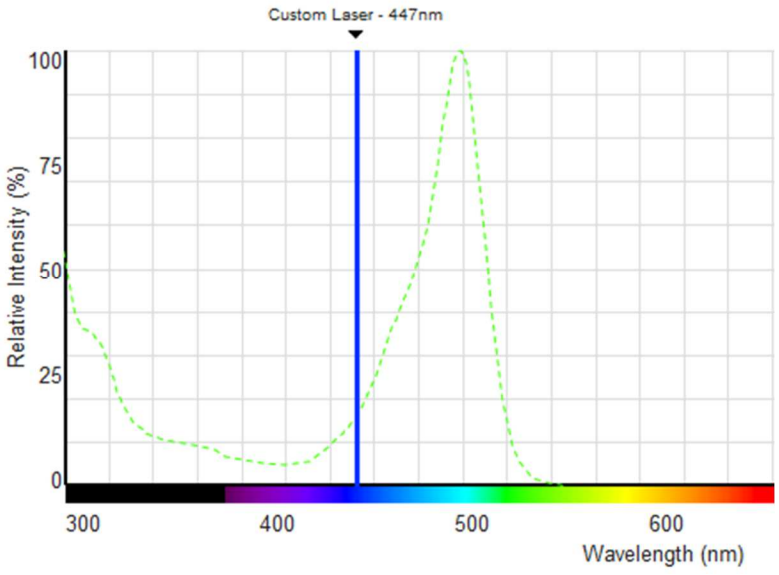

Figure 11. Fluorescein perchlorate excitation spectra ("Life Technologies Fluorescence SpectraViewer", n.d.)

The fluorescein derivative, Fluorescein sodium salt ($C_{20}H_{10}Na_2O_5$), was a suitable, better replacement for Fluorescein perchlorate with use with the 447nm laser. According to Sigma-Aldrich, Fluorescein sodium salt has an optimal excitation wavelength at 460nm, which will produce a significantly greater fluorescence signal with the 447nm laser. Also, since the fluorescein derivative is a salt, it is soluble in water. Furthermore, the derivative is safe to use in the laboratory and cost effective, costing only $30 for 100g.

Fluorescein sodium salt has an optimal emission wavelength at 515nm. The optimal emission wavelength differs from that of the excitation wavelength by over 30nm, therefore negligible amounts of the excitation light will influence the emission/fluorescent light taken from the DPLIF system with an adequate bandpass filter. The bandpass filter chosen for the Fluorescein sodium salt was an Andover Corporation 514.5nm filter with a FWHM of 10nm. A 10nm FWHM filter was chosen over the narrower 2nm FWHM filter originally used to allow adequate fluorescent light in so that the Nikon cameras could detect the fluorescence. Since the optimal emission wavelength is more than 30nm away from the excitation wavelength, the increased filter range will not be affected by the excitation photons.

Oxazine725 has an optimal excitation wavelength at 646nm and optimal emission wavelength at 661nm, displayed in Figure 12 (Fluorophores.org, n.d.). Therefore, the 655nm laser excites oxazine close to optimal intensity. However, Oxazine725 has a low quantum yield producing a low fluorescent intensity, which was apparent in the optimization tests, as shown in

Figure 13. In the image, it is difficult to differentiate a defined spray structure compared to Figure 14, where the fluorescent Oxazine750 was used.

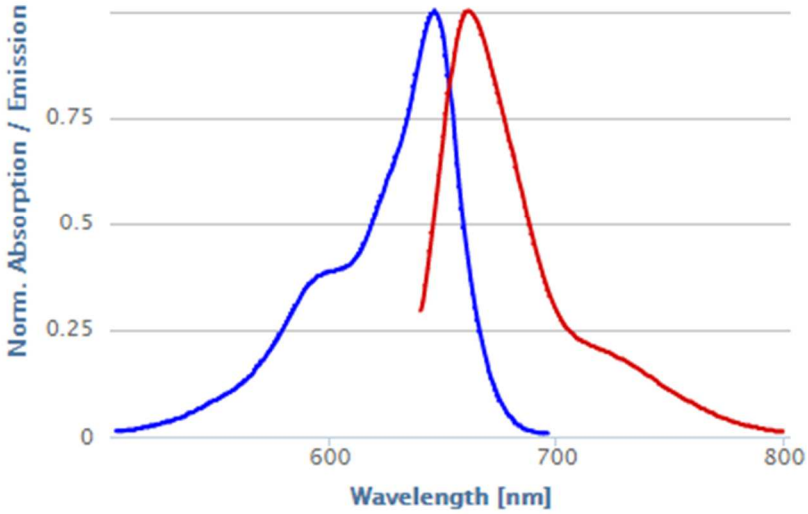

Figure 12. Oxazine725 excitation spectra (blue) and emission spectra (red) (fluorophores.org, n.d.)

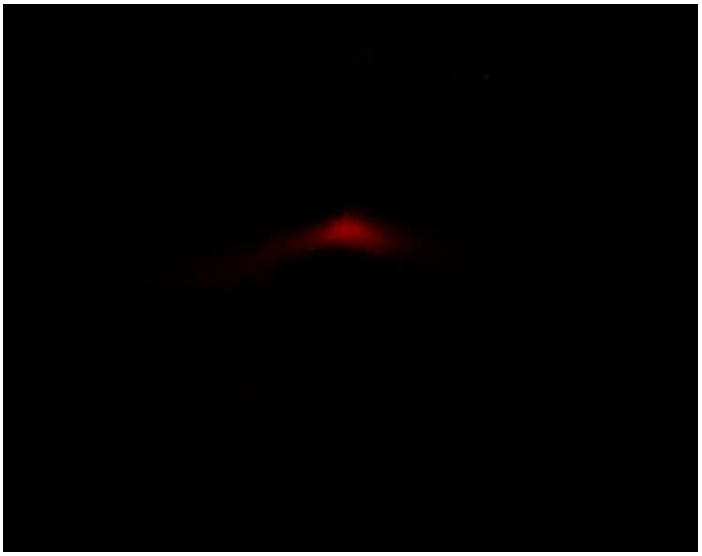

Figure 13. Oxazine725 image in optimization spray test

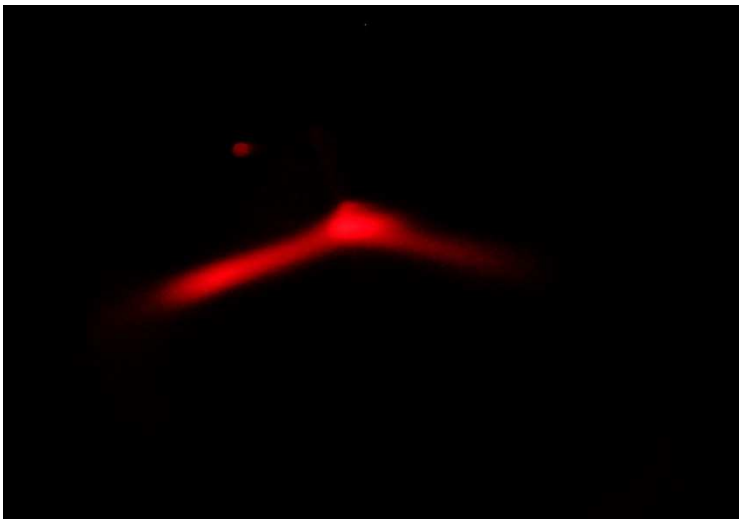

Figure 14. Oxazine750 image in optimization spray test

Oxazine750 has similar excitation and emission spectra with an optimal excitation wavelength at 665nm and an optimal emission wavelength at 678nm, as shown in Figure 15 ("Oxazine750", n.d.). Although Oxazine750 has similar excitation and emission spectra as Oxazine725, Oxazine750 has a different chemical structure than Oxazine725. The chemical structure of Oxazine725 and Oxazine750 are displayed in Figure 16 and Figure 17, respectively. Oxazine750 has a total of three aromatic rings, where oxazine725 has two aromatic rings. More intense fluorescence is found in compounds containing aromatic rings due to the low energy $\pi \rightarrow \pi^*$ transitions. Nitrogen heterocyclic groups by themselves do not fluoresce due to an $n \rightarrow \pi^*$ transition. However, when nitrogen heterocyclic groups are fused to other aromatic rings, there is an increase in molar absorptivity of the absorption band and the fluorescence is observed (Wong, D., n.d.). Oxazine725 and Oxazine750 both have one nitrogen heterocyclic group, however oxazine750 has three aromatic groups fused to the nitrogen heterocyclic group, compared to two in oxazine725. Therefore, oxazine750 will have a larger quantum yield and was deemed good choice for the DPLIF system.

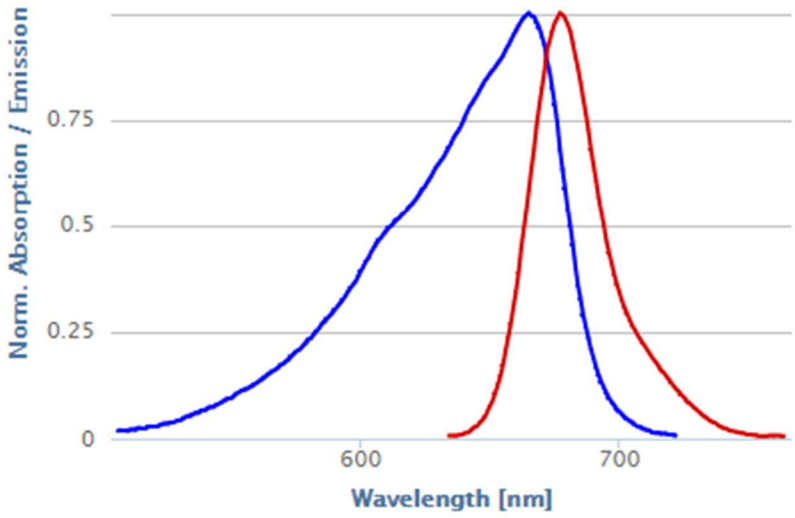

Figure 15. Oxazine750 excitation spectra (blue) and emission spectra (red) (fluorophores.org, n.d.)

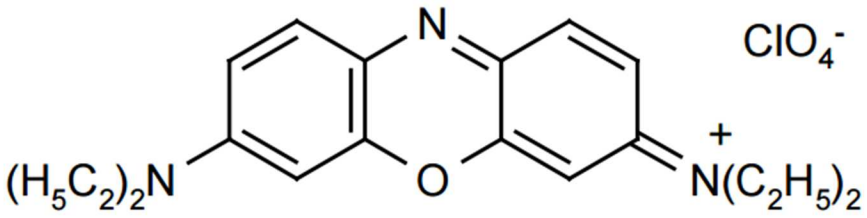

Figure 16. Oxazine725 chemical structure

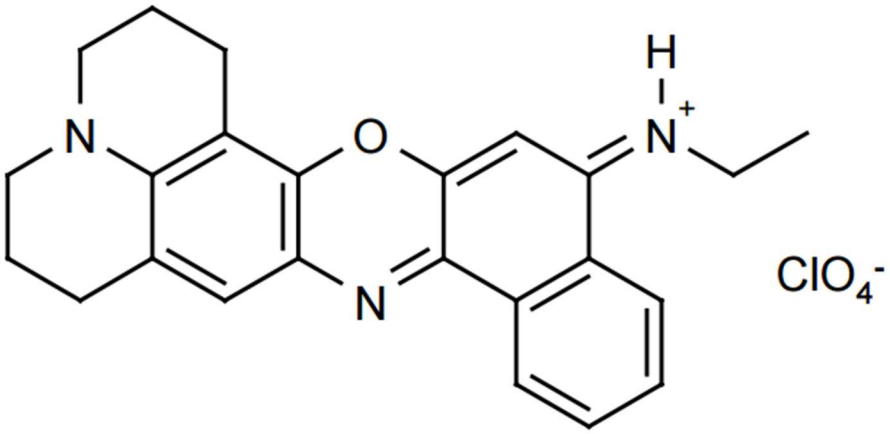

Figure 17. Oxazine750 chemical structure

A 680nm bandpass filter with a FWHM of 10nm was chosen for oxazine750. Since the 680nm bandpass filter is 25nm away from the 655nm excitation wavelength, negligible amounts of the excitation light will influence the emission/fluorescent light taken from the DPLIF system and therefore, this filter was considered suitable for the DPLIF system.

4.1.2 Scattering Efficiency Dependence on Wavelength

Scattering efficiency factors of spherical droplets depend on the complex refractive index and the ratio of the particle's radius to wavelength (Kokhanovsky, 2016). Therefore, the scattering efficiency is dependent on the wavelength used. Since two different wavelengths are used in the DPLIF system at the same time, it is important to understand whether one wavelength affects the results of the other and vice versa. Therefore, the scattering efficiencies of both the 447nm and 655nm lasers were determined. In order to determine the scattering efficiency dependence on wavelength, a Malvern spray distribution was analyzed using a Rosin-Rammler distribution function, which then was coupled to the Mie scattering data produced from Light Lab software. Coupling the calculated Mie scattering extinction coefficients with the size distribution allowed for the calculation of the extinction coefficient for each wavelength (447nm and 655nm) at each tested X-axis position within the tested spray to be calculated. Finally, ratios of the calculated extinction coefficients for each laser were compared and the dependence of wavelength on scattering efficiency was determined.

To study the droplet size distribution of the spray, a Malvern RTS-5113 laser system was used. Data was taken using unlike doublet injectors at a 90° impingement angle and a constant Z-axis position, 60mm downstream from the impingement point, and Y-axis position, with varying X-axis positions ranging from -6.000mm to 6.000mm by increments of 2.000mm, with the X-position 0.000mm at the impingement point, as displayed in Figure 18. A MATLAB tool, created

by Ivan Brezani, et.al., (2010) was then used to transform the Malvern Gaussian size distribution to fit a Rosin-Rammler distribution function.

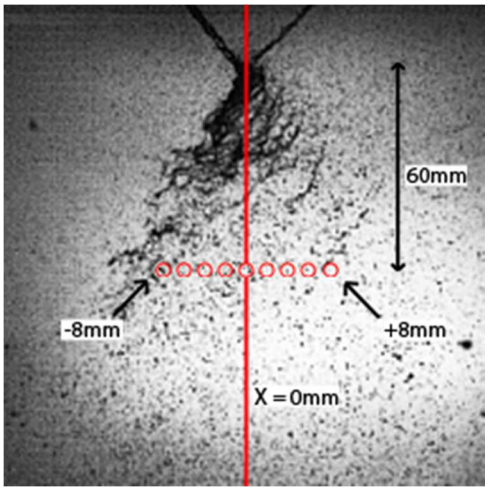

Figure 18. Malvern measurement schematic

In order to model the Mie scattering of the spray, the imaginary part of the index of refraction was determined. In order to determine the imaginary part of the index of refraction, the absorption coefficient was measured. The absorption coefficient for each wavelength was found from tests performed using the 447nm and 655nm lasers that make up the DPLIF system. Two calibration curves were constructed, one for each laser used.

A series of solutions of differing concentrations of oxazine750 in water and fluorescein sodium salt in water were prepared for the 655nm and 447nm calibration curves, respectively. The oxazine and fluorescein solution concentrations tested are displayed in Table 2.

Table 2. Fluorescein and oxazine concentrations used for the calibration curves.

Fluorescein solutions (µM)	Oxazine solutions (µM)
3	2
5	3
10	5
15	10
20	15
-	20

For each concentration, the solution was placed in a quartz cuvette 6mm from the laser. A power meter was placed behind the cuvette and recorded the intensity of the light exiting the cuvette, as displayed in the experimental schematic shown in Figure 19. The initial intensity of each laser was recorded via the power meter in the absence of the cuvette. Furthermore, a "blank", containing deionized water, was measured before each data point was collected for each laser.

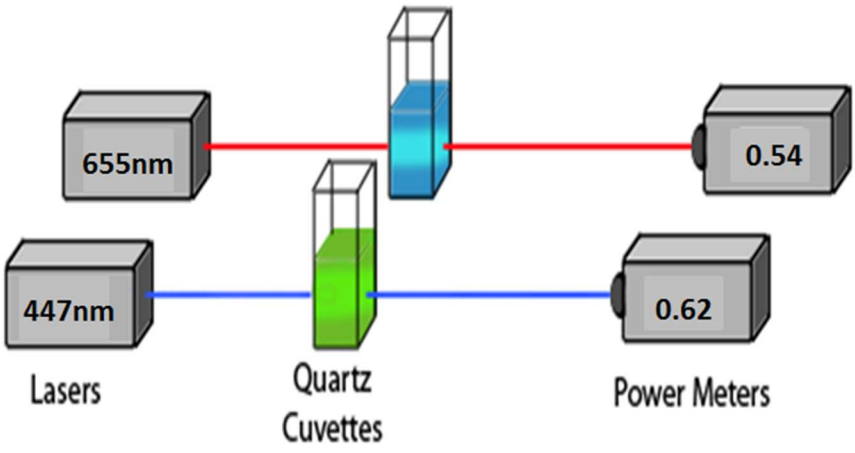

Figure 19. Laser system schematic for the creation of the fluorescein and oxazine calibration curves.

The calibration curves were then constructed from the data points collected. Two additional calibration curves with the same solutions were created using a Shimadzu UV-1700 Spectrometer. The UV-Vis spectrometer calibration curves were then used in comparison with the laser induced fluorescence (LIF) curves to determine the accuracy and precision of the LIF calibration curves. Then, using the calibration curves and Beer's Law, the molar absorption coefficient was determined for both oxazine and fluorescein.

Calibration curves to determine the molar absorption coefficient of both the 447nm laser with differing concentrations of fluorescein and the 655nm laser with differing concentrations of oxazine were constructed. Figure 20 displays the oxazine calibration curve from the LIF system with concentrations ranging from 2µM to 20µM.

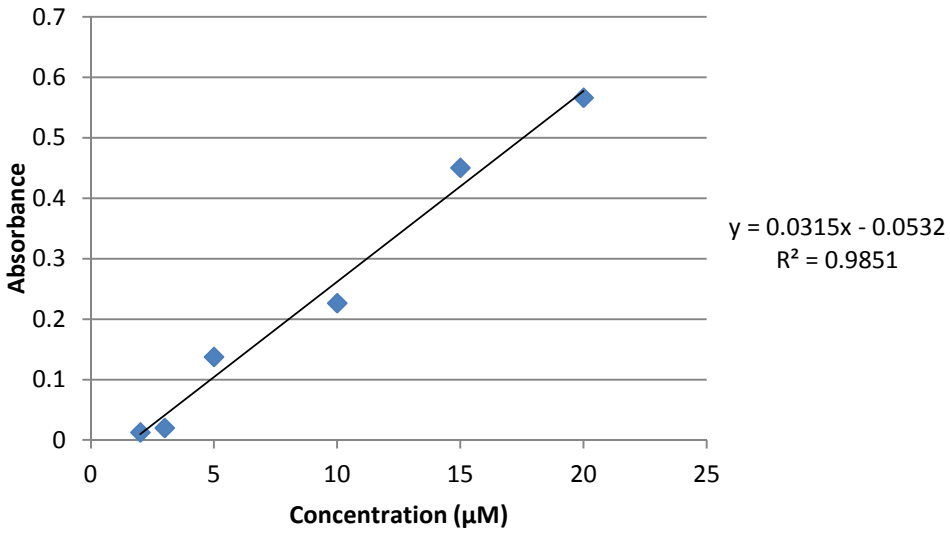

Figure 20. Laser induced fluorescence calibration curve for oxazine.

The molar absorption coefficient (slope) was determined to be 0.0315$\mu M^{-1}cm^{-1}$. The molar absorption coefficient was then multiplied by the concentration of oxazine in the oxidizer fluid (20µM) to produce an absorption coefficient, equal to 0.63 cm^{-1}.

An additional calibration curve was constructed using the Shimadzu UV-1700 Spectrometer to determine the precision and accuracy of the LIF systems. The UV Vis spectrometer calibration curve for oxazine is displayed in Figure 21.

The UV Vis spectrometer calibration curve for oxazine exhibits a molar absorption coefficient equal to 0.0355 $\mu M^{-1}cm^{-1}$, which differs from that of the LIF system by 11.27%.

Figure 22 displays the fluorescein calibration curve from the LIF system with concentrations ranging from 3µM to 20µM. The molar absorption coefficient (slope) was determined to be equal to 0.0178$\mu M^{-1}cm^{-1}$. The molar absorption coefficient was then multiplied by the concentration of fluorescein in the fuel fluid (20µM) to produce an absorption coefficient, equal to 0.356 cm^{-1}.

An additional calibration curve was constructed for the fluorescein solutions using the UV Vis spectrometer, which is represented in Figure 23. The UV Vis spectrometer calibration curve for fluorescein depicts an absorption coefficient equal to 0.0193 $\mu M^{-1}cm^{-1}$, which differs from that of the LIF system by 7.78%.

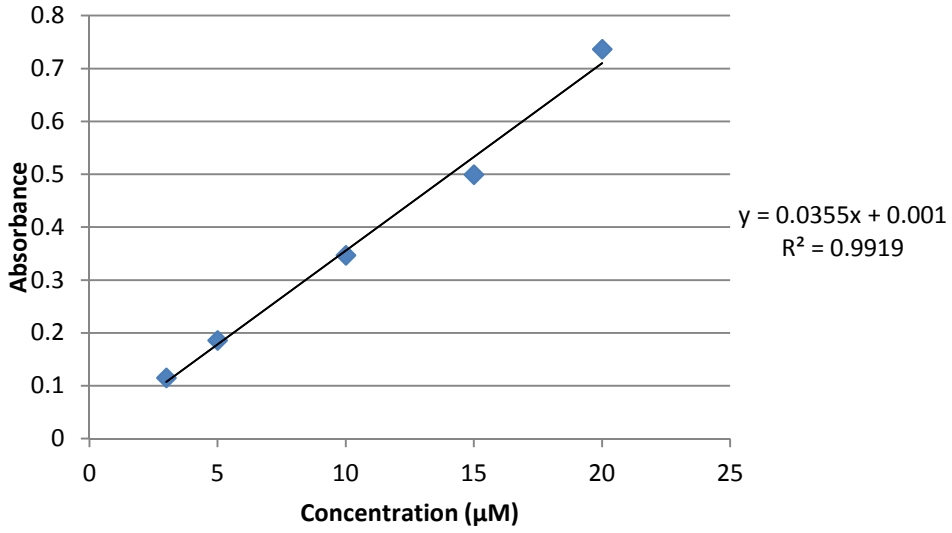

Figure 21. UV Vis spectrometer calibration curve for oxazine.

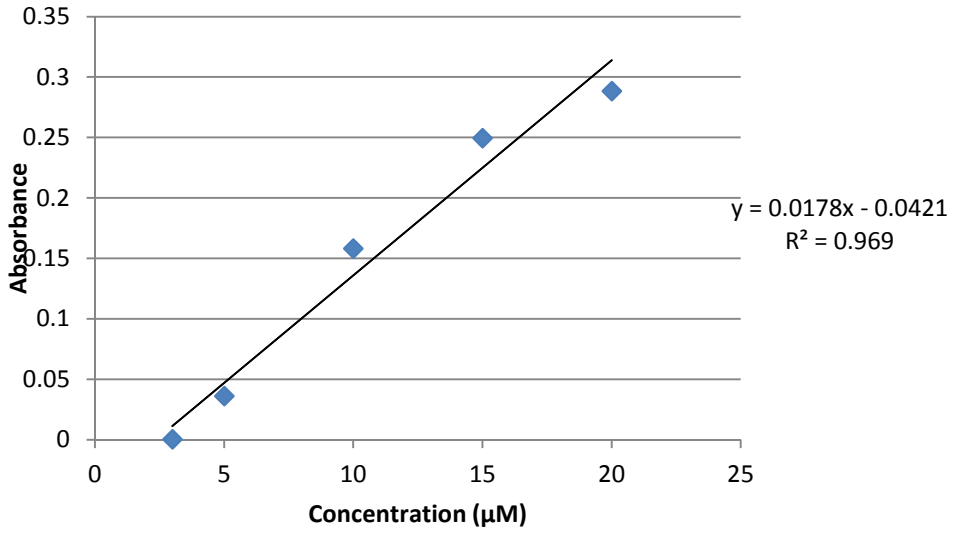

Figure 22. LIF calibration curve for Fluorescein.

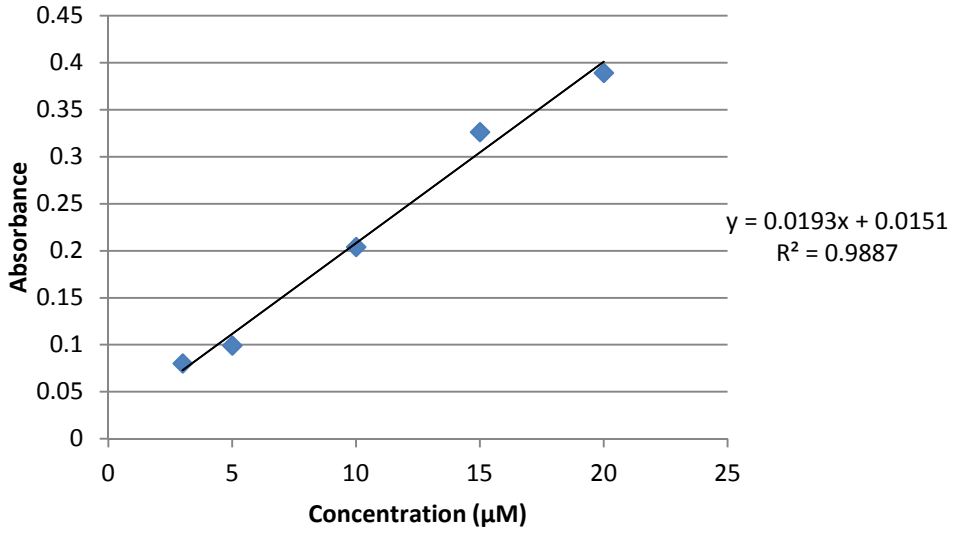

Figure 23. UV Vis spectrometer calibration curve for fluorescein.

The determined absorption coefficients for both the oxazine and fluorescein experiments were used in the imaginary part of the index of refraction calculations. The absorption coefficient for each wavelength is related to the imaginary part of the index of refraction through the equation

$$\gamma^{-1} = \frac{\lambda}{4\pi n'} \qquad \textbf{Equation 4}$$

where γ is the absorption coefficient, λ is the laser wavelength and *n'* is the imaginary part of the index of refraction (Lefebvre, 1999; Van De Hulst, 1981).

The imaginary part for 447nm and 655nm were determined via Equation 4 and are displayed in Table 3, along with the other parameters used for the Mie Scattering calculations.

Table 3. Parameters used for Mie scattering calculations

Parameter	Value
Droplet Diameter	Variable
Range of Droplet Diameter	2.0 to 300 µm
Index of Refraction-Real Part	1.33
Index of Refraction-Imaginary Part (oxazine)	3.83×10^{-6}
Index of Refraction-Imaginary Part (fluorescein)	4.90×10^{-7}
Wavelength of Beam	0.447µm, 0.655µm
Beam Waist Diameter	1.00E6 µm
Scattering Angle	0.00 Degrees
Number of Data Points	1500
Imaginary part (447nm)	1.26×10^{-10}
Imaginary part (655nm)	3.28×10^{-10}

The calculated Mie scattering results from the Light Lab software were then coupled with the Malvern distribution data that was transformed using a Rosin-Rammler distribution function to determine the extinction coefficients for each laser at the X-axis positions tested. The ratio of

the calculated 447nm and 655nm extinction coefficients at the varying X-axis positions are displayed in Table 4.

Table 4. Calculated extinction coefficient ratios (447nm/655nm)

X-axis Position (mm)	Impingement Angle (degrees)		
	50	**70**	**90**
-6	0.998	0.997	0.997
-4	0.997	0.998	0.997
-2	0.997	0.997	0.997
0	0.997	0.997	0.997
2	0.997	0.997	0.997
4	0.998	0.997	0.997
6	0.997	0.997	0.997
8	0.997	0.997	0.997

Furthermore, experimental data was collected to confirm the calculated scattering efficiency dependence on wavelength and is displayed in Table 5. The initial intensity (I_0) of each laser was measured via a power meter. Then the incident intensity of the laser beam after it traveled through the spray plume (I) was measured. The I_0/I at each X-axis position were calculated and the two lasers were then compared to each other.

Table 5. Experimental extinction coefficient ratios (447nm/655nm)

X-axis Position	Extinction Coefficient Ratio (447nm/655nm)
-6	1.04
-4	0.99
-2	0.99
0	0.99
2	0.98
4	1.01
6	0.98

Based on the data collected and analyzed, all three impingement angles tested display ratios close to 1.0 for all X-axis positions tested. Based on these results, no correction factor is needed to account for the differences in scattering efficiency when using different wavelength lasers.

4.1.3 Camera Selection

Cameras used for PLIF applications have varied since the 1980s when the PLIF technique was developed. Grayscale cameras are favored for PLIF. Grayscale sensors allow photons of any wavelength into the tiny photosites (light cavity), thus producing a grayscale image because the photosites are unable to distinguish the amount of each color present. Color sensors place filters for specific wavelengths (colors) of photons above each photosite, permitting only certain colors of light to enter each cavity, which allows for color selectivity, producing an RGB image ("Digital Camera Sensors", n.d.). Therefore, color sensors have high selectivity, but lower sensitivity ("Color Versus Black",n.d.). Since liquid sprays produce small droplets, generating a weaker fluorescence signal per volume compared to stationary fluoresced fluids, higher sensitivity is desirable and grayscale camera sensors are more favorable for low intensity PLIF experiments. However, the camera chosen for each PLIF system depends on the experiment being run due to the trade-off between maximizing frame rate, intensity and clarity of the image. Therefore, for the DPLIF optimization, shutter speed, ability to capture fluorescent intensity and overall image clarity were taken into account along with camera cost and camera software integration abilities.

To choose an optimal camera, understanding what can affect the fluorescence intensity in the image and overall resolution of the image is vital. In the 1990s, CCD cameras were introduced into PLIF systems. In 1990, Prasad and Sreenivasan performed experiments using a

PLIF system with a 12-bit CCD camera chip (Prasad and Sreenivasan, 1990). The bit-depth determines the intensity resolution, where if a CCD camera has a bit-depth equal to N, the maximum discrete grayscales it can have is 2^N (Crimaldi, 2008). Therefore, the 12-bit camera chip will have 4096 discrete grayscales.

Additionally, pixel count is an important factor in camera selection due to the fact that it highly influences spatial resolution (Crimaldi, 2008). PLIF experiments done by Bruchhausen et al. (2005) used a camera with a pixel count of 1376 x 1224 to produce higher spatial resolution in their images compared to experiments performed with sensors that have lower pixel counts, such as the experiments performed by Van Vliet et al. (2004).

Furthermore, the spectral sensitivity of the camera is an important factor due to its influence on image resolution. The sensitivity of the CCD chip influences the required exposure time of the camera to produce a higher resolved image (Crimaldi, 2008). Some researchers, such as Crimaldi and Koseff (2001) used a Dalstar SMD-1M15 CCD camera with an aperture of 14.3mm x 14.3mm. Since PLIF systems use flat laser sheets where the laser light is not concentrated in a local area, but spread throughout the spray, a large aperture is needed in PLIF systems. Also, since narrow band filters are placed in front of the camera, letting even less light reach the CCD chip, larger apertures allow for more light to enter allowing the fluorescence to be visible in the image.

In recent years, Intensified Charge-Coupled Device (ICCD) cameras have been used in LIF and PLIF systems, instead of normal CCD cameras due to some advantages to using ICCD cameras over CCD cameras. Previous experiments performed with the DPLIF setup by Sung (2014) used an Andor iStar ICCD camera. The Andor ICCD camera is designed for rapid, time-

resolved imaging that is ideal for PLIF based experiments. The Andor camera uses image intensifiers and high resolution CCD sensors, as displayed in Figure 24, to create time-resolved images even at very low lighting and fluorescent intensity ("The iStar ICCD", n.d.). Although the light intensifying capability of ICCD cameras is ideal for PLIF systems, the cost of an ICCD camera can range from $40,000 to $70,000, which is a major disadvantage when optimizing the system. Therefore, non-intensified CCD cameras were sought as a possible cost effective option for the optimization of the DPLIF system.

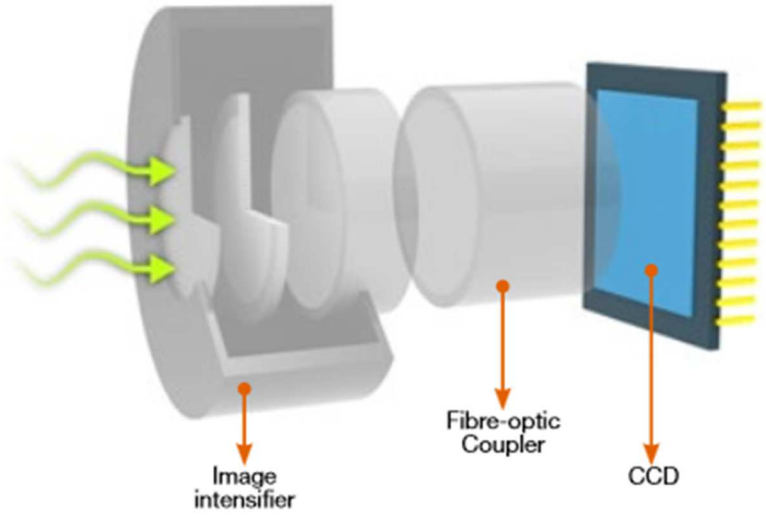

Figure 24. Andor iStar ICCD camera schematic. ("Andor iStar ICCD", n.d.)

To help further optimize the cost of the DPLIF system, it was thought that webcams or scientific CCD cameras could be used instead of commercialized CCD cameras. However, multiple software programs and camera integration into LabView would need to be completed for webcam use in DPLIF experiments. Furthermore, webcams are not meant to be used for image capture, but rather continuous streaming. Therefore, camera software to capture images and change exposure and aperture settings on a webcam would need to be developed. Lastly, Nikon SLR camera lenses and sensors are more sensitive to light than webcams, therefore it is

expected that a consumer CCD camera will ultimately produce better quality images than a webcam. Consequently, although webcams would be more cost effective, they would not be more time effective and may not produce high quality images. Furthermore, scientific CCD cameras would produce higher quality images and may be more compact than consumer CCD cameras; however scientific CCD cameras are more expensive than consumer cameras. Therefore, consumer cameras were chosen for the imaging optimization of the DPLIF system.

When taking shutter speed, ability to capture fluorescent intensity, overall image clarity, cost and camera software integration abilities into account, it was found that a Nikon D90 camera with the Nikon AF-S Nikkor 18-105mm f/3.5-5.6G ED lens was suitable for the DPLIF system. The relevant technical specifications of the Nikon D90 are displayed in Table 6. In comparison to the cameras used in past experiments listed above, the Nikon D90 has a sensor size of 23.6mm x 15.8mm, which is greater than that of the SMD-1M15 used in the Crimaldi and Koseff experiments (2001), leading to a higher number of pixels to collect light particles on the sensor and thus, a higher sensitivity. With a large CCD sensor, the Nikon D90 has a maximum image size of 4,288 x 2,848 pixels, which is over three times that in the camera used in the Bruchhausen et al. experiments ("D90 Specifications", n.d.). Additionally, the Nikon D90 is equipped with a color CCD sensor and although the color sensor uses a Bayer color filter array, which places a color filter on each pixel of the sensor to selectively choose colors, the Nikon D90 has over three times the number of pixels as the camera used in the Bruchhausen et al. experiments (2005). Therefore, the spatial resolution of the Nikon D90 will be higher than that of the camera used in the Bruchhausen et al. experiments.

The sensor size also plays an important role when determining the depth of field a given camera will have. As the sensor size increases, the depth of field will decrease for a given

aperture (“Digital Camera Sensors”, n.d.). Therefore, smaller aperture sizes need to be used in order to maintain the same depth of field of smaller sensors. In order to maintain the required depth of field using the Nikon D90 camera and the Nikon AF-S Nikkor 18-105mm f/3.5-5.6G ED lens, an aperture of f/4.5 was used throughout the duration of the experiments. Overall, larger sensors generally provide more control over the quality of the image. This flexibility allows for a comparable depth of field and to a smaller sensor without reducing the quality of the image by using a higher ISO, increasing the sensor’s sensitivity to light, and smaller aperture (“Digital Camera Sensors”, n.d.).

Table 6. Nikon D90 specifications

Specification	range
Aperture	f/3.5-f/36
ISO	200-6400
Shutter speed	¼,000- 30sec
Sensor size	23.6mm x 15.8mm
Image size	4,288 x 2,848 pixels
Bit-depth	12-bit

To determine if the Nikon D90 will work sufficiently with the DPLIF system, the aperture, ISO and shutter speed were tested and optimized using a spray representative of those for which the diagnostic is intended to be applied to. For the D90 settings optimization tests, two unlike-doublet injectors were used. One injector discharged “fuel” containing 20uM of fluorescein sodium salt and the other discharged “oxidizer” containing 20uM of oxazine750. Throughout all the doublet injector tests, purified water was used as both the fuel and oxidizer.

The oxidizer and fuel injector orifices had diameters of 0.5842mm and 0.4267mm, respectively. The area of the oxidizer and fuel nozzles were $2.68e^{-7}$ m^2 and $1.4e^{-7}$ m^2, respectively, where the discharge coefficient was assumed to equal 1. The fluorescein injector was set to a mass flow rate of 12lb/hr and the oxazine injector was set to 12lb/hr. Furthermore, the camera had a 680nm -10nm bandpass filter attached to the camera to capture the fluorescence of oxazine excited by the 655nm laser. Further camera tests were performed to capture the fluorescence of fluorescein excited by the 447nm laser and a 515nm-10nm bandpass filter attached to the camera.

Figure 25 displays a zoomed in doublet injector spray model to better depict the DPLIF images. The D90 settings optimization tests demonstrated an optimal fluorescence intensity and image resolution for doublet injector sprays using a f/4.5 aperture, a hi0.3 (4000) ISO and a 15 second shutter speed. An aperture of f/4.5 was chosen as the optimal aperture for the doublet injectors' spray a few reasons. When changing the zoom of the lens, the aperture will change. As the zoom was increased from 18mm to 35mm, the aperture increased from f/3.5 to f/4.5. When f/4.2 or lower was used a "light ring" appears in the final image for oxazine, as shown in Figure 26. This ring could be due to light entering the camera lens between the lens-to-filter step-down ring and the bandpass filter. By increasing the zoom, the aperture number increases, and the amount of light allowed into the camera lens decreases. At an aperture of f/4.5, the "light ring" no longer appears, as displayed in Figure 27. At a zoom larger than 35mm (a larger aperture than f/4.5) the fluoresced spray image becomes more granular and blurry. Therefore, f/4.5 was deemed suitable for the DPLIF system.

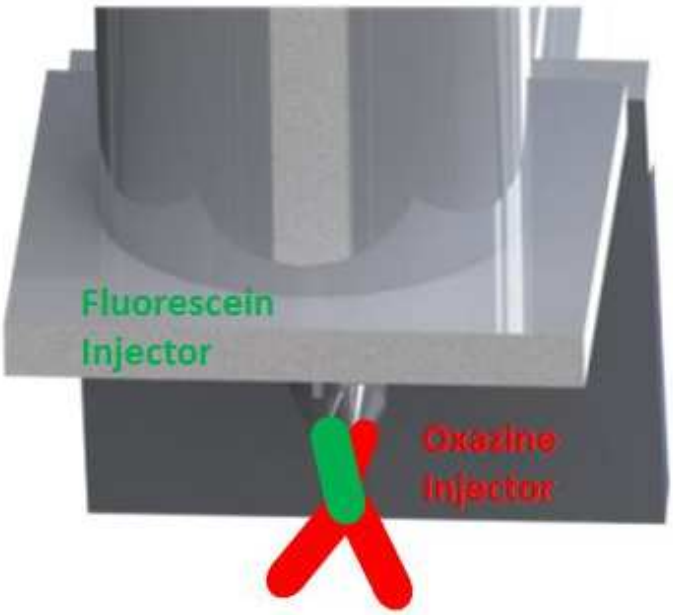

Figure 25. Doublet injector optimization experiment model

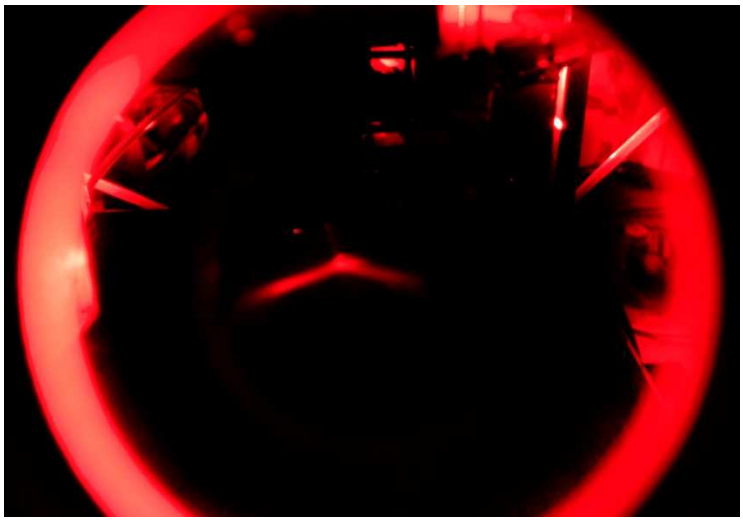

Figure 26. Oxazine spray image with an f/3.5 aperture

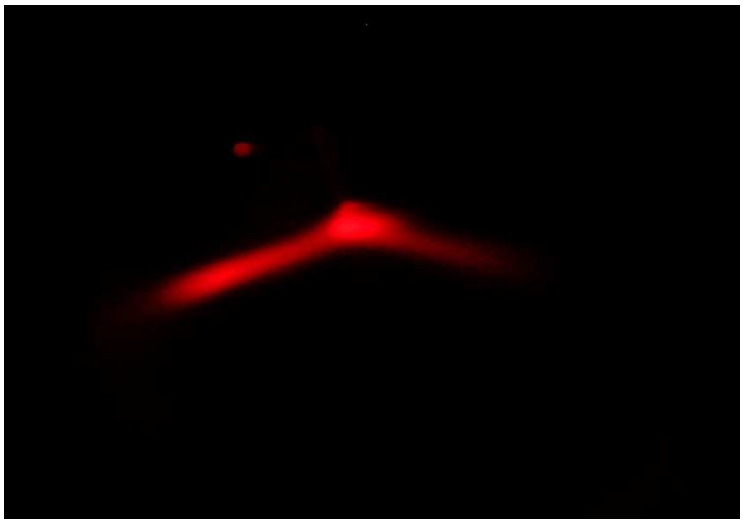

Figure 27. Oxazine spray image with an f/4.5 aperture

Figure 28 displays the color image of oxazine taken by the Nikon D90 at the optimal settings and Figure 29 displays the same image transformed into grayscale. It was found that the grayscale value (0-255) for the fluoresced parts of the image reached a maximum of 83, while the dark sections of the image registered on the gray scale at values around 10. Therefore, after signmal calibrations are performed with a known fluorescence source, matlab image processing codes will be able to distinguish from fluoresced pixels and background pixels, allowing for DPLIF data analysis of sprays using a Nikon CCD camera with the settings mentioned above. Lastly, the Nikon D90 costs around $450, where the Andor iStar CCD camera costs over $40,000. Thus, using the Nikon D90 camera drastically reduces the cost of the DPLIF system, ultimately increasing its cost-performance.

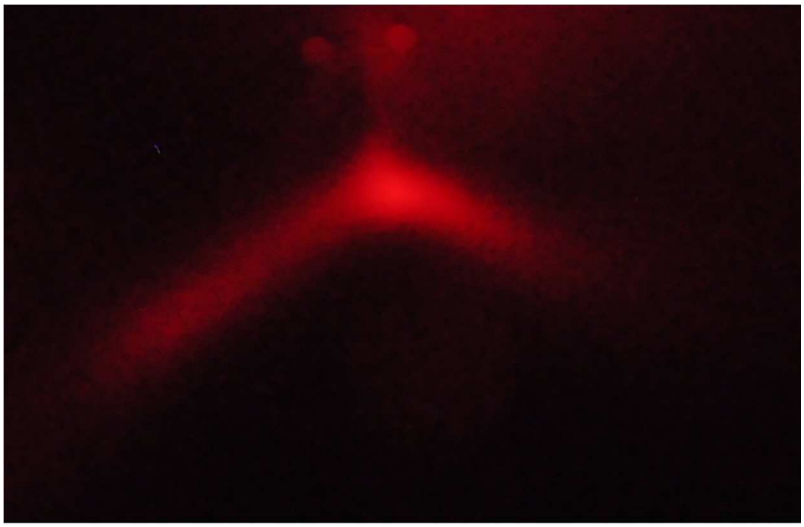

Figure 28. Color cropped fluorescent Nikon D90 image

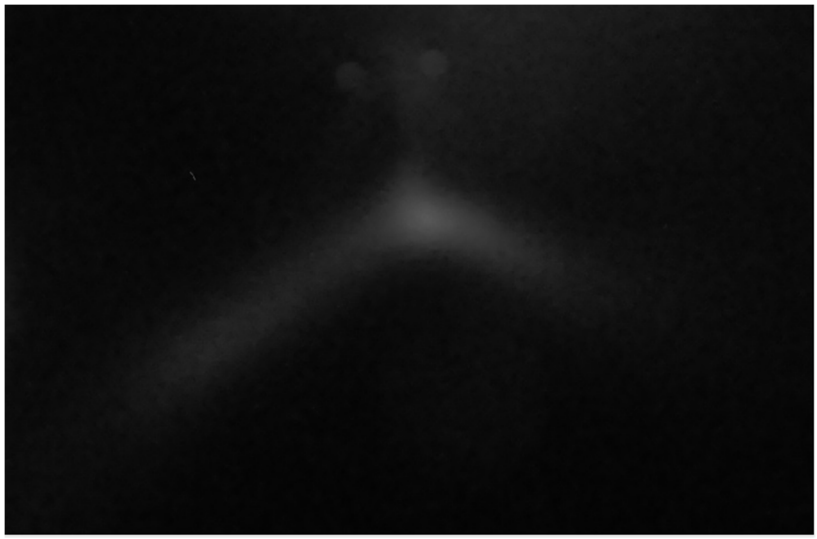

Figure 29. Grayscale cropped fluorescent Nikon D90 image

In previous uses of the DPLIF system, only one camera was used to determine the concentration/intensity of the fuel and oxidizer solutions (Sung, 2014). When only one camera is used, only one liquid can be studied at a time because only one fluorescent bandpass filter can attach to the camera lens at a given time. This setup can lead to experimental errors because the fluorescence of both the fuel and the oxidizer in the spray cannot be measured at the same time.

Although the spray is thought to remain constant throughout the tests, this is not always the case. Therefore, to mitigate this instrumental error, either an image splitter with one camera or two cameras that trigger at the same time can be used. The OptoSplit II image splitter would be ideal for the optimization of the DPLIF system; however it costs over $10,000 and therefore, is not cost effective. Also, such a system will immediately halve the pixel resolution of each image. Consequently, the two camera option was chosen. Two Nikon D90 cameras were used and were triggered at the same time, by an infrared signal sent from a Nikon ML-L3 wireless remote control, when used in the DPLIF system.

The two camera system still required the ability to isolate the two fluorescents. This was accomplished through a combination of mirrors. The light first passed through a Thor labs dichroic mirror with a 550nm cutoff wavelength. The mirror reflects 100% of the light between 350nm and 540nm and transmits 100% of the light between 560nm and 850nm, as shown in Figure 30 (Thor Labs, n.d.). Therefore, light at wavelengths under 540nm will be detected by camera 1 and light at wavelengths above 560nm will be detected by camera 2. The reflected light was then redirected by a standard 2'' square protected aluminum mirror to Camera 2. Further light filtering occurred as the light passed through the 10nm bandpass filter on each camera. Camera 1 detected the fluorescence of oxazine and camera 2 detected the fluorescence of fluorescein, as depicted in Figure 31. Figure 31 depicts the combined fluorescence as the magenta arrow, the fluorescence of oxazine as the red arrow and the fluorescence of fluorescein as the blue arrow.

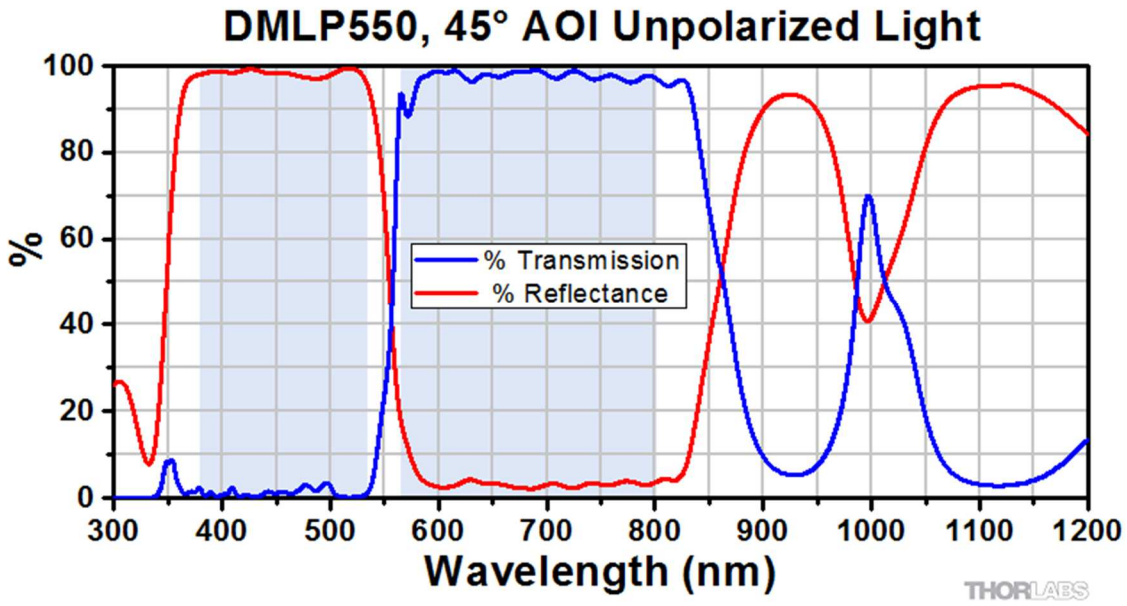

Figure 30. Transmittance and reflectance plot of the 550nm dichroic mirror (Thor labs, n.d.)

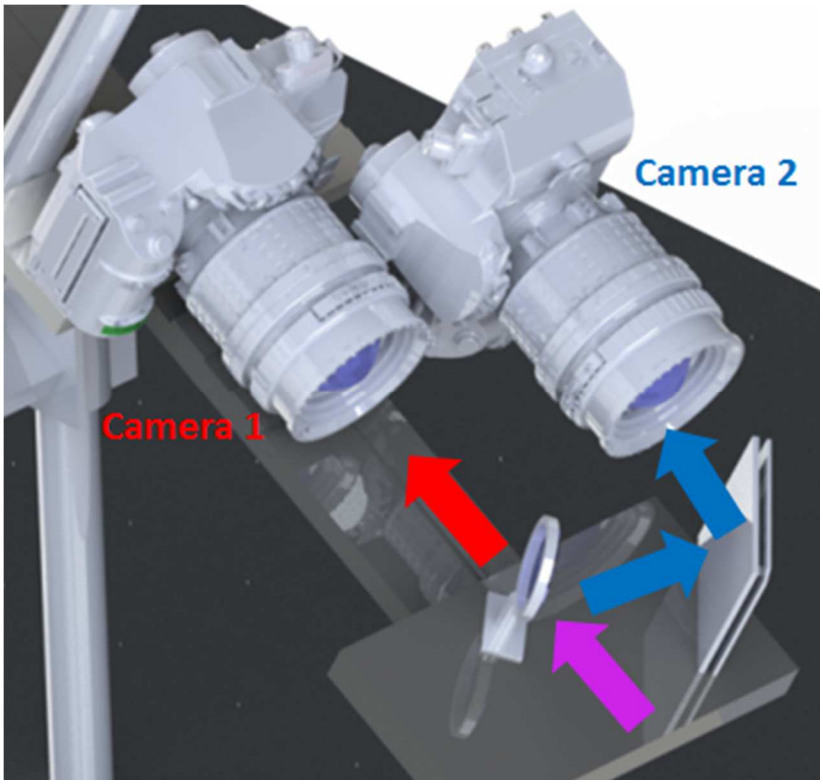

Figure 31. Camera system fluorescence separation

4.1.4 Optomechanical Enhancements

In previous experiments performed by Bolszo (2011) and Sung (2014), a series of lenses were used to match the focus and divergence of both the 447nm and 655nm, ensure beam intensity and correct for beam differences. Although the original DPLIF setup functioned, there were some disadvantages to account. The original optical setup led to constant instrumental errors and inconsistent data. Also, the original setup was not compact or ideal for commercialization. Therefore, a series of improvements were made to increase the planar reliability of the DPLIF system and to decrease the size of the overall system.

Each beam from the two diode lasers was collimated at the laser exit using an Opto Engine 400um multimode fiber coupler with an SMA905 connector. The fiber couplers were then attached to an Ocean Optics Split400-UVVIS 400um fiber splitter/combiner. Using the combiner, the 447nm and 655nm beams were combined to a single fiber. A 40mm collimating lens was then used at the end of the fiber to collimate both beams together which then passed through a cylindrical lens to form a planar sheet. An achromatic lens was then used to further collimate the planar sheet and to help ensure consistent planar thickness and intensity in the x and y-directions of the spray. The x-direction and y-direction spanned from -40mm to 40mm with the middle of the testing rig and the focal point of the achromatic lens at the 0mm position. Figure 32 displays the test stand arrangement for the beam power tests. Figure 33 displays a Gaussian distribution for the plane intensity measurements in the x-direction of the spray. The Gaussian distribution is expected and due to the inclusion of an achromatic lens to the DPLIF system. Figure 34 displays very little change in the laser plane power as the distance from the focal point changes in both the negative and positive direction.

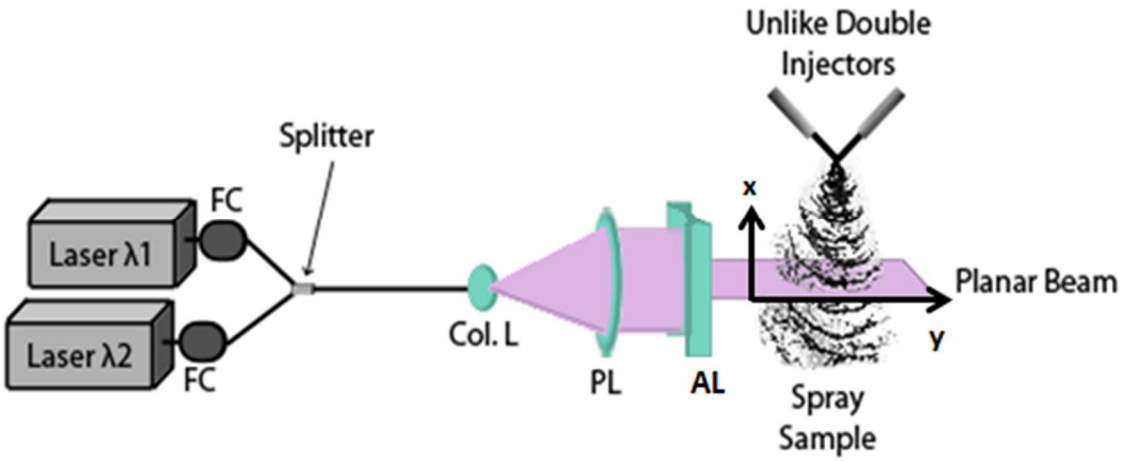

Figure 32. DPLIF power meter test schematic

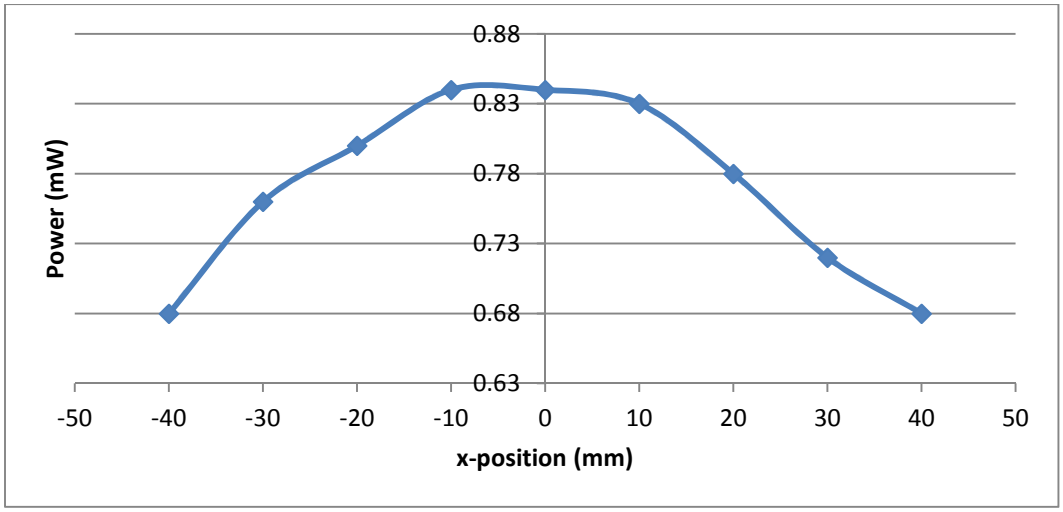

Figure 33. Laser plane intensity in the x-direction for the DPLIF

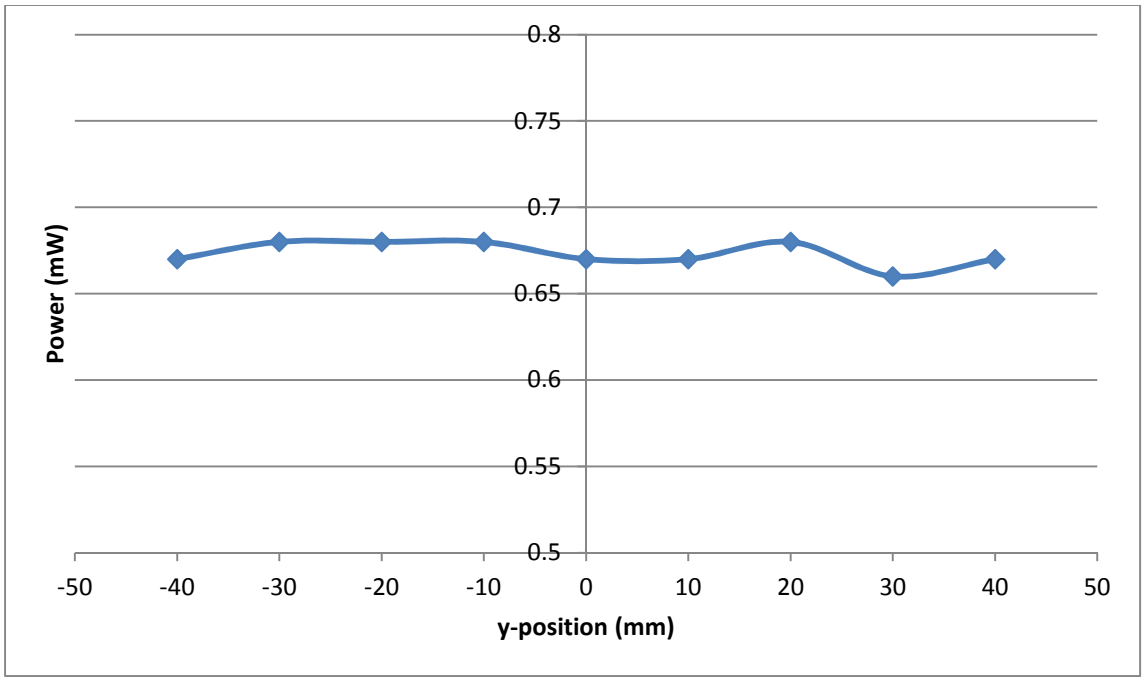

Figure 34. Laser plane intensity in the y-direction for the DPLIF

The increase in the planar stability of the DPLIF system is due to the fiber coupling of the lasers and the addition of an achromatic lens. Tests performed with the original DPLIF setup displayed inconsistent and irregular planar intensities in both the x and y-directions. Therefore, the addition of an achromatic lens and the fiber coupling instead of lenses has improved the optic setup of the DPLIF instrument, leading to more consistent and reliable data.

4.1.5 Image Registration Code

A Matlab program was developed to analyze the DPLIF system images accurately and efficiently. In order to determine the relative concentration of fuel and oxidizer in a specified area of the spray, a composite of the oxazine and fluorescein images needed to be produced and the fluorescent intensities needed to be compared. To optimize the code and test its functionality, optimization tests using the unlike doublet injectors were performed. For the preliminary code optimization tests, one Nikon D90 camera was used. Oxazine and fluorescein spray images were taken with the sprays both at 20µM concentrations and 10lb/hr flow rates. First, the oxazine filter

was attached to the camera and data was taken for the fluorescence of the oxazine, then the filter was changed to the fluorescein filter and fluorescein data was acquired. The position of the camera would remain unchanged for the duration of the tests. Furthermore, the spray would be maintained at a constant flow rate.

The oxazine and fluorescein 4,288 x 2,848 pixel .JPG images produced by the Nikon D90 camera were then imported and "read" via the Matlab program. The minimum and maximum coordinate values in the x and y-dimensions were transposed into the "world coordinate system", specified as a two-element numeric vector, for each image using the Matlab function "WorldLimits". Once the coordinate system of each image was established, the Matlab image analysis function "imfuse" was used to create a composite of the two images and analyze the relative intensities of each fluorescent. Imfuse first created a composite image from the two images, where the output is a numeric matrix containing a fused version of the two input images. The imfuse function incorporated the raw images and the spatial information associated with the input of the images. Furthermore, the imfuse function contains a method where the subfunction "falsecolor" was used to create a composite RGB image showing the two images overlain in different color bands. The "Scaling" and "joint" subfunctions scale the intensity values in the images jointly as if they are in the same image. The intensity similaries and differences within the composite image were displayed from the "ColorChannels", where red signifies areas intensity in the oxazine image, green signifies areas of intensity in the fluorescein image and yellow signifies areas of similar intensity where both are present in the same region ("Mathworks: Imfuse", 2012). Figure 25 displays a model of the spray interactions presented in Figure 35, an analyzed composite image taken from the preliminary optimization tests with one camera.

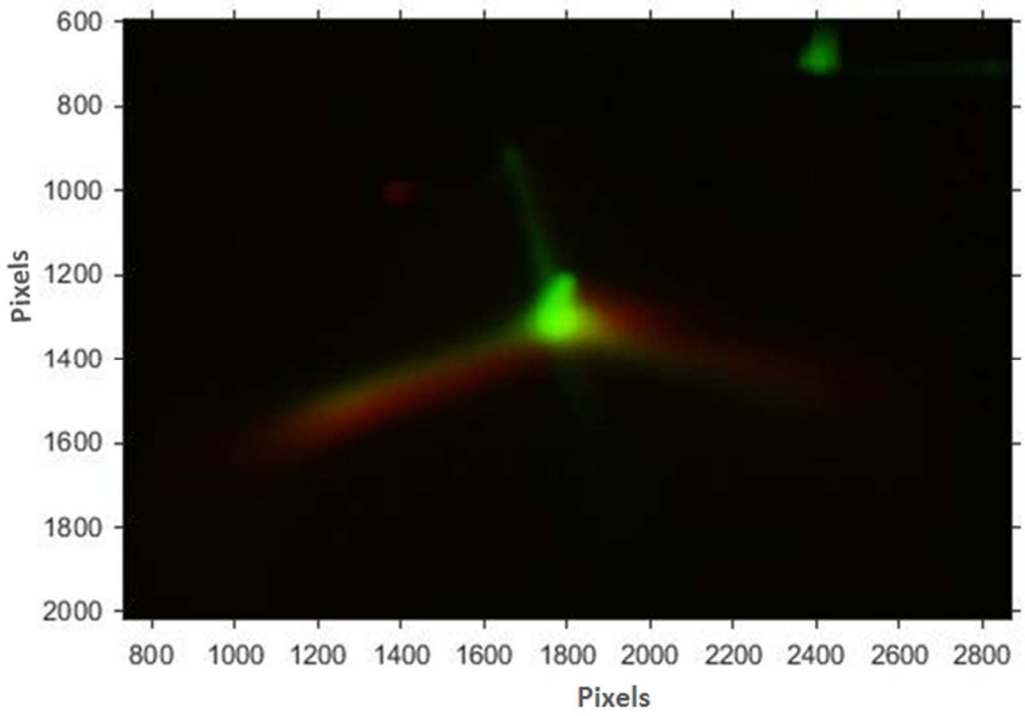

Figure 35. Matlab code optimization test composite image

With use of the imfuse Matlab function, the original image analysis code used was drastically reduced in size. The working Matlab code used to analyze the DPLIF images throughout this thesis is a total of eleven lines of code, which can be found in Appendix A. This optimized Matlab code has ultimately reduced the analysis time and has provided a more visual representation of the collected data.

4.2 Instrument Integration

The DPLIF instrumentation is comprised of three component systems: the laser system, the optics system and the camera system. Figure 36 below displays a condensed block diagram of the DPLIF system with a "sample" component consisting of the liquids of interest. For example, the "sample" component could be a single drop, liquid solutions, such as a stream of fluids or liquids in cuvettes, or a spray.

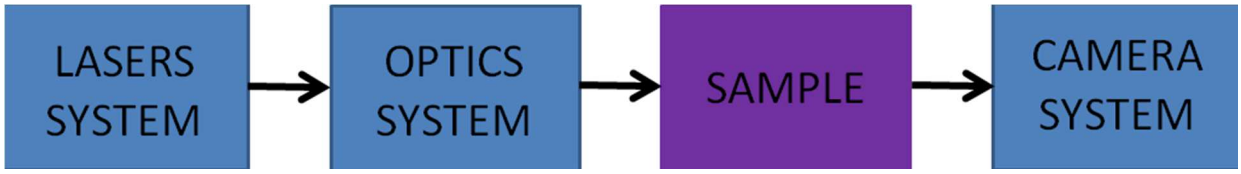

Figure 36. DPLIF instrumentation block diagram

The optimized DPLIF laser system is comprised of a 447nm and a 655nm two Watt solid state OEM Laser Systems lasers. The optimized optics system is also comprised of two Opto Engine 400um multimode fiber couplers with SMA905 connectors, one connected to each laser, and an Ocean Optics Split400-UVVIS 400µm Fiber splitter/combiner. Furthermore, the optical system contained a 40mm collimating lens that was then used at the end of the fiber to collimate both beams together which then passed through a cylindrical lens to form a planar sheet. An achromatic lens was the last component of the optical system and was used to further collimate the planar sheet. Figure 37. depicts the DPLIF laser and optical system.

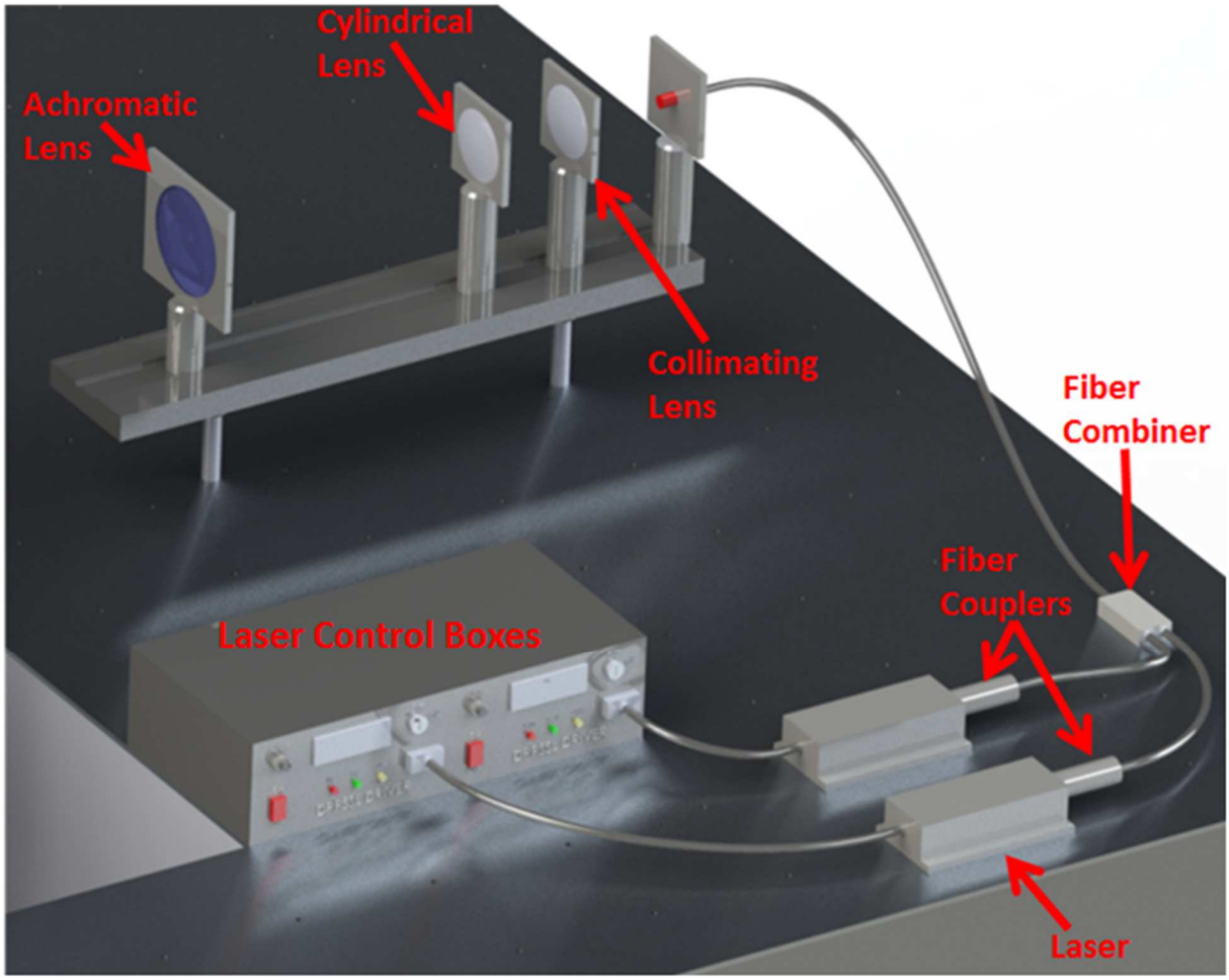

Figure 37. Laser and optical system model

The DPLIF sample system consists of a compartment to hold the analyzed liquid, such as a cuvette, or a liquid generator, such as a single drop generator or fuel injector. The optimal fluorescents for the DPLIF sample system were determined to be Oxazine750 and Fluorescein sodium salt. Oxazine750 and Fluorescein sodium salt had larger quantum yields than the previously used fluorescents. Furthermore, the concentrations of each fluorescent used in the liquid samples were 20μM for both oxazine and fluorescein for the optimization and proof of concept tests. Figure 38 depicts the experimental setup for the unlike doublet injector experiments tested, which is an example of the three sample systems tested. The other two

sample systems tested were a cuvette stationary liquid sample system and a simplex nozzle spray sample system.

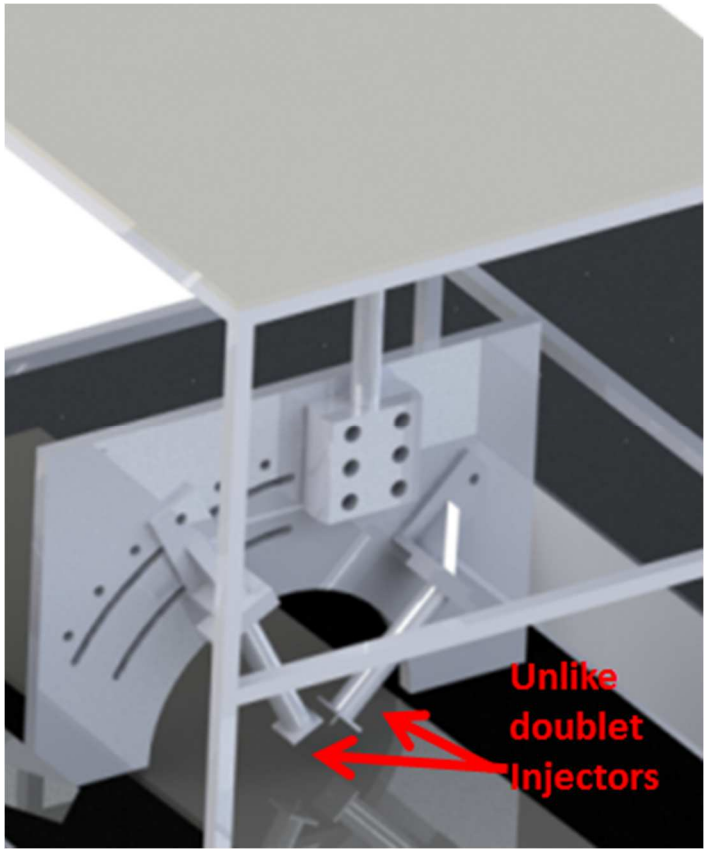

Figure 38. Unlike doublet injector spray sample system

The camera system was comprised of two Nikon D90 cameras with the Nikon AF-S Nikkor 18-105mm f/3.5-5.6G ED lenses. The camera system was also comprised of Andover Corporation 514.5nm and 680.0nm filters with a FWHM of 10nm, a Thor labs 550nm dichroic

mirror and a 2” square aluminum protected mirror, as displayed in

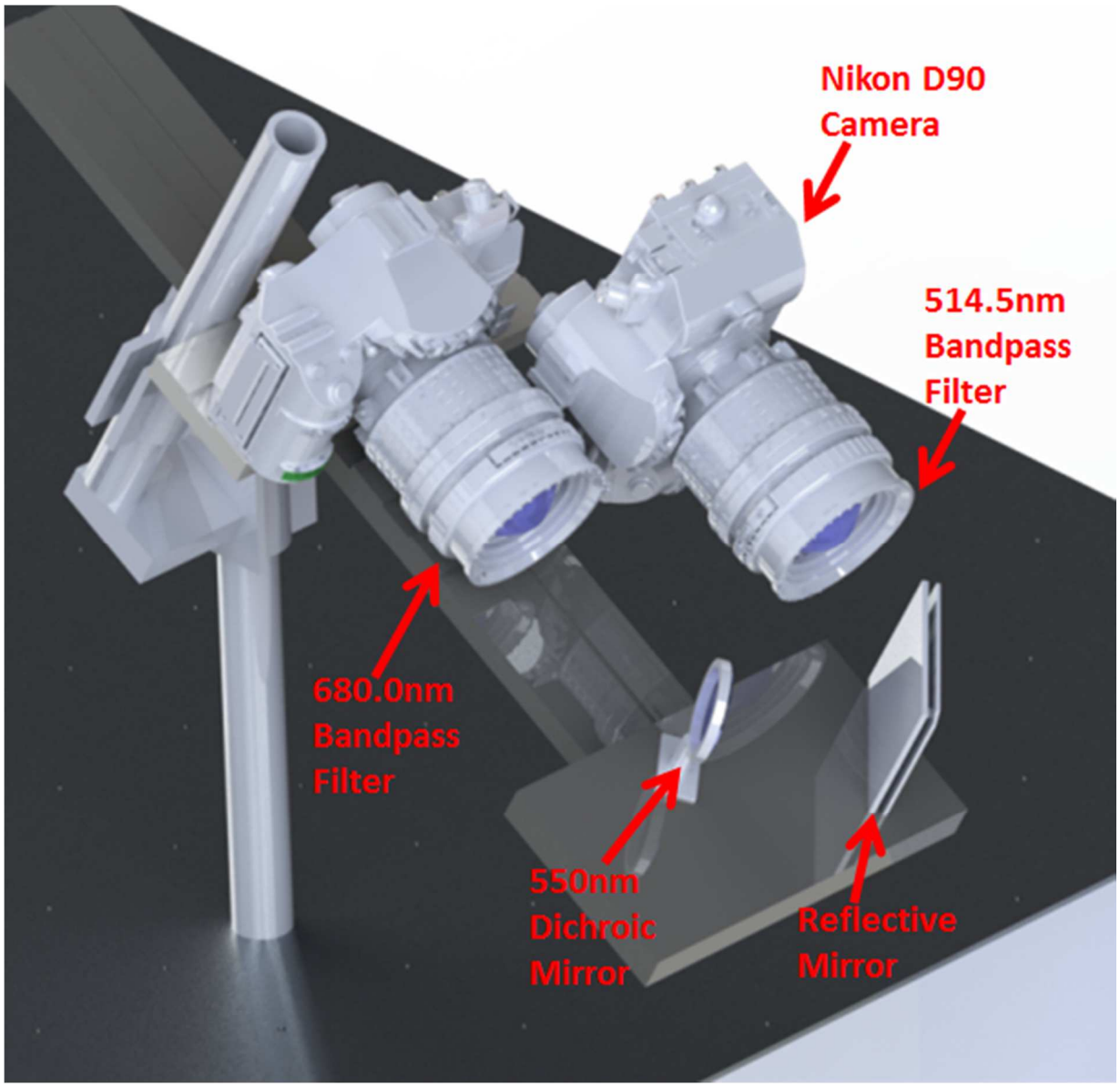

Figure 39. The fluorescent light hit the dichroic mirror at a 45° angle, where wavelengths above 550nm would be transmitted by the filter and wavelengths below 550nm would be reflected towards the aluminum protected mirror. The incorporation of the dichroic mirror along with the fluorescent specific bandpass filters ensured that the intended fluorescent light was analyzed by each camera, respectively.

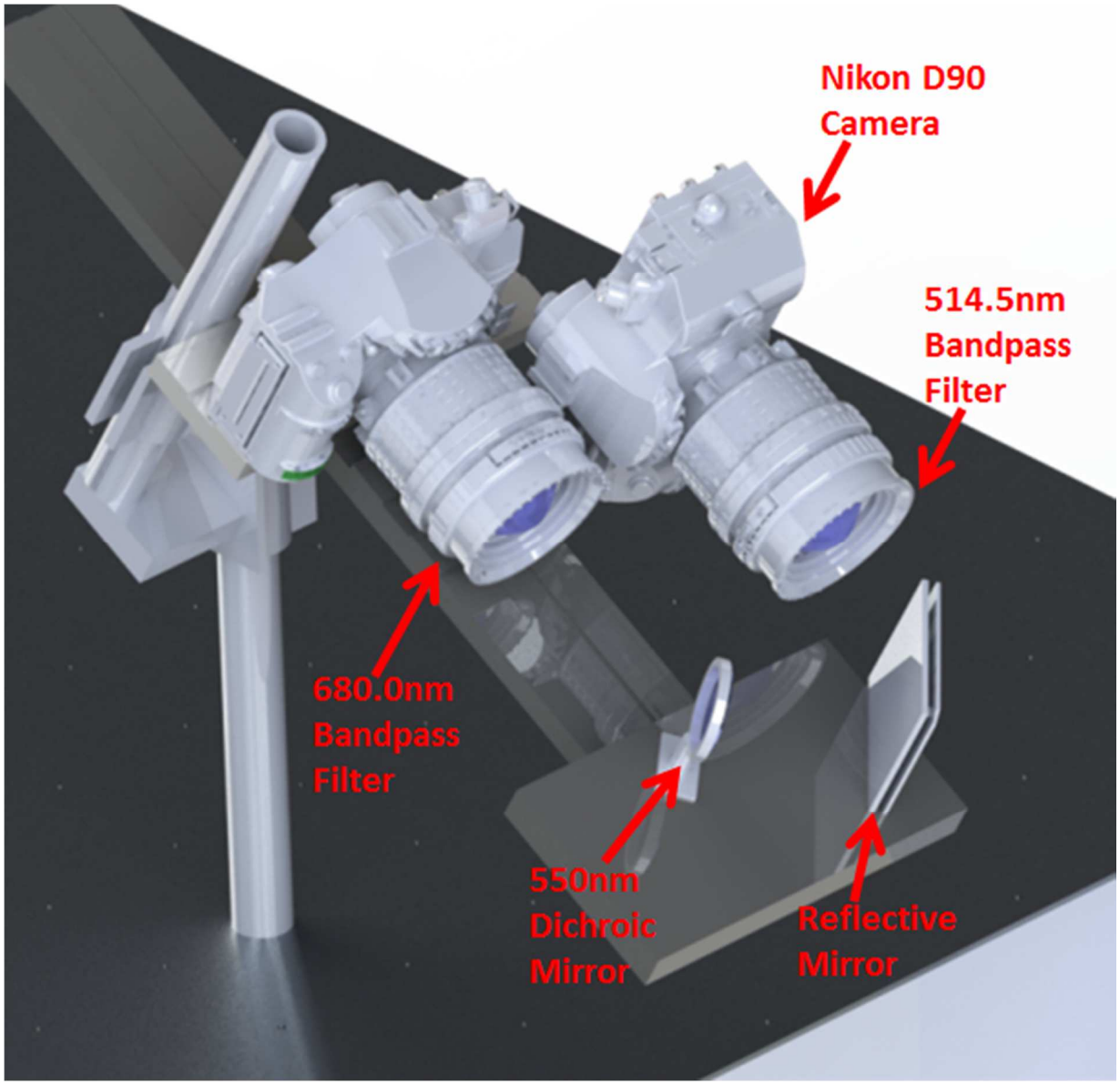

Figure 39. Camera system model

The complete optimized DPLIF system, with the doublet injector sample system is depicted below in

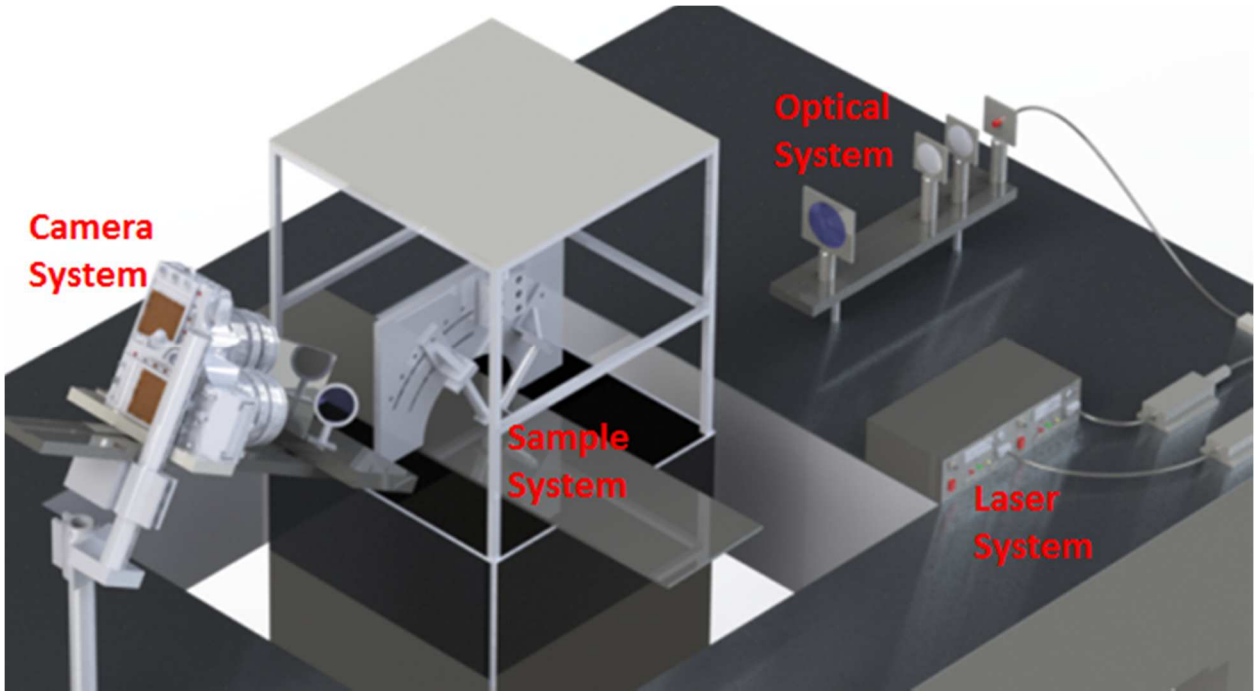

Figure 40. The complete DPLIF system can fit on a four square meter test stand. The optimized system represented below was used for the remainder of the experiments tested in the study.

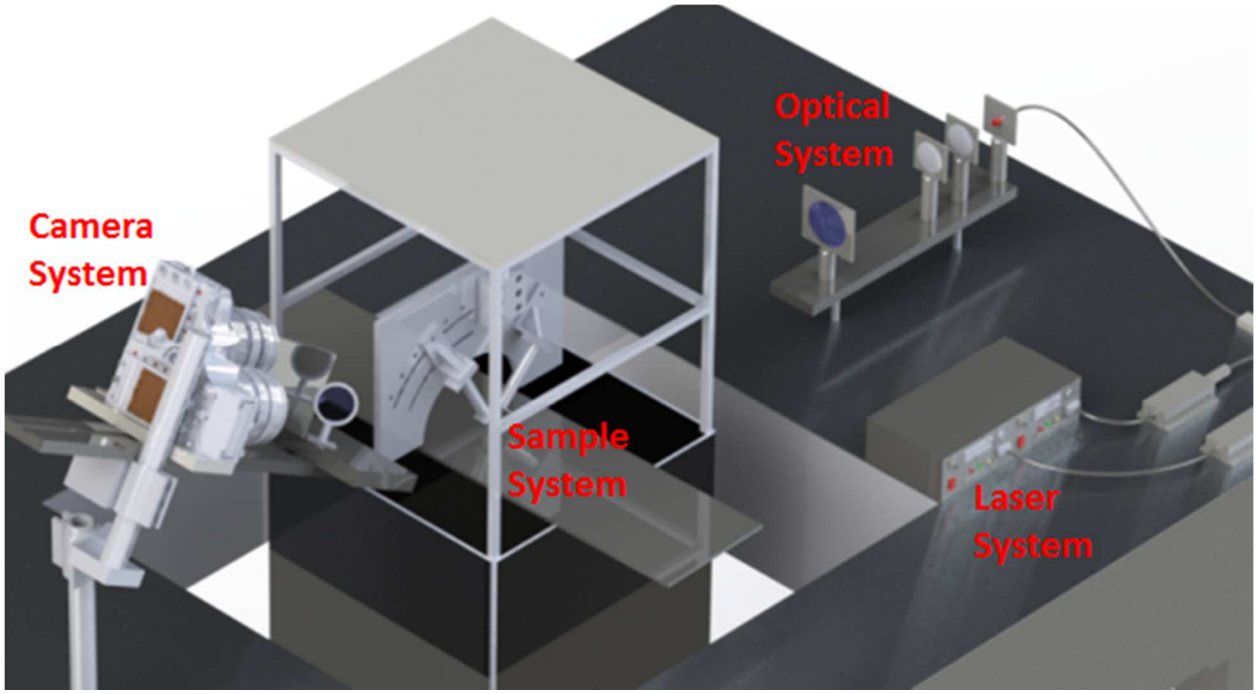

Figure 40. DPLIF system model

4.3 DPLIF Applications

A series of proof of concept experiments were conducted to test the functionality and use of the optimized DPLIF system. Cuvette experiments were performed to determine the functionality of the DPLIF system for analysis of standing liquids. Spray experiments were also performed to determine the ability of the DPLIF system to analyze the interactions of two liquids in a dynamic environment. For the spray experiments, data of fuel and oxidizer interactions was collected from both a simplex and unlike doublet injectors.

4.3.1 Cuvette Experiments

To determine the DPLIF functionality and performance in the analysis of standing liquids, a series of cuvettes with differing concentrations of oxazine solution and fluorescein solutions were tested. In the experiment, three cuvettes were used, one containing 100% oxazine solution (20μM), the second containing 50% oxazine-50% fluorescein solution and the third containing 100% fluorescein solution (20μM). The three cuvettes were aligned in a row so that

the DPLIF laser sheet penetrated all three cuvettes (where the direction of the laser sheet is displayed as the magenta arrow coming out of the cuvettes/page) at the same time, as displayed in Figure 41. The figure displays the 100% fluorescein solution by volume in the left cuvette, the 50-50 mixture by volume in the middle cuvette and the 100% oxazine solution by volume in the right cuvette.

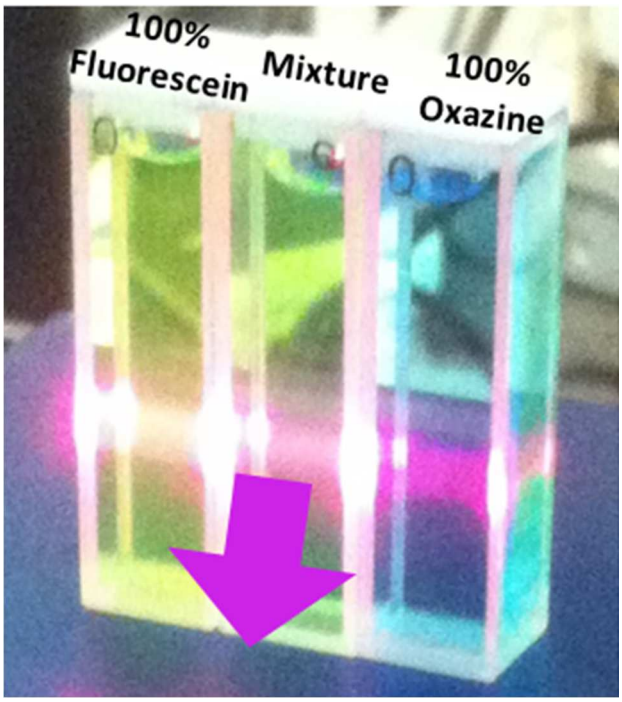

Figure 41. Cuvette experimental setup

In order to determine if the DPLIF system can accurately assess a 50-50 mixture of two interacting liquids, the resulting composite image should display similar intensity representing similar volumes of liquid present in that given area. The laser power, ISO and shutter speed needed to be adjusted so that the 100% solutions displayed the same intensity and did not saturate their respective camera sensor. This technique was used as a way to normalize the two fluorescents since fluorescein has a higher quantum yield than oxazine. If fluorescein is naturally more fluorescent than oxazine and is kept at the same laser and camera settings as oxazine, the DPLIF data analysis will indicate the fluorescein solution is more predominant in every location

that fluorescein and the oxazine solution interact. Therefore, by initially equaling the fluorescein and oxazine fluorescence when they are separate, some potential experimental errors can be minimized. The optimized laser current (power), camera ISO and camera exposure time were determined and displayed below in

Table 7. Optimal parameter settings for cuvette experiments

Fluorescent of Interest	Laser Current (Amps)	Camera ISO	Camera Exposure Time (seconds)
Oxazine	2.11	Hi0.3	0.5
Fluorescein	0.33	Lo0.3	0.5

Take note that the laser power and camera ISO for fluorescein are significantly lower than that of oxazine in order to get similar fluorescence intensities. Fluorescein has a higher intensity compared to that of oxazine at similar laser and camera settings due to fluorescein having a higher fluorescence quantum yield and that the color sensor in the Nikon D90 uses a Bayer color filter array. In a Bayer color filter array there are twice as many green sensors as there are red or blue. This is because the human eye is more sensitive to green light than red and blue light, thus redundancy with green pixels produces an image which appears less noisy and has finer detail than if the color sensors were equally distributed throughout the sensor ("Digital Camera Sensors", n.d.). Since the fluorescein fluorescence signal produces a green color captured by the camera, the analyzed fluorescein signal may be influenced by the structure and use of the Bayer filter array. Therefore, in order to equalize the fluorescence signal captured by the color sensors in the Nikon D90 cameras, the laser power and camera ISO settings for fluorescein are considerably lower than that of oxazine throughout the tests.

It is also important to note that the optimal parameters used for each laser and camera varies between experiments and concentrations of fluorescent used. Therefore, these settings should be determined before the primary experiment is run in order to "blank" the system before analyzing liquid mixtures.

Once the system had been "blanked", the 50-50 mixture was analyzed using the working Matlab code. The original images produced by each camera and the resulting composite image are displayed below in Figure 42.

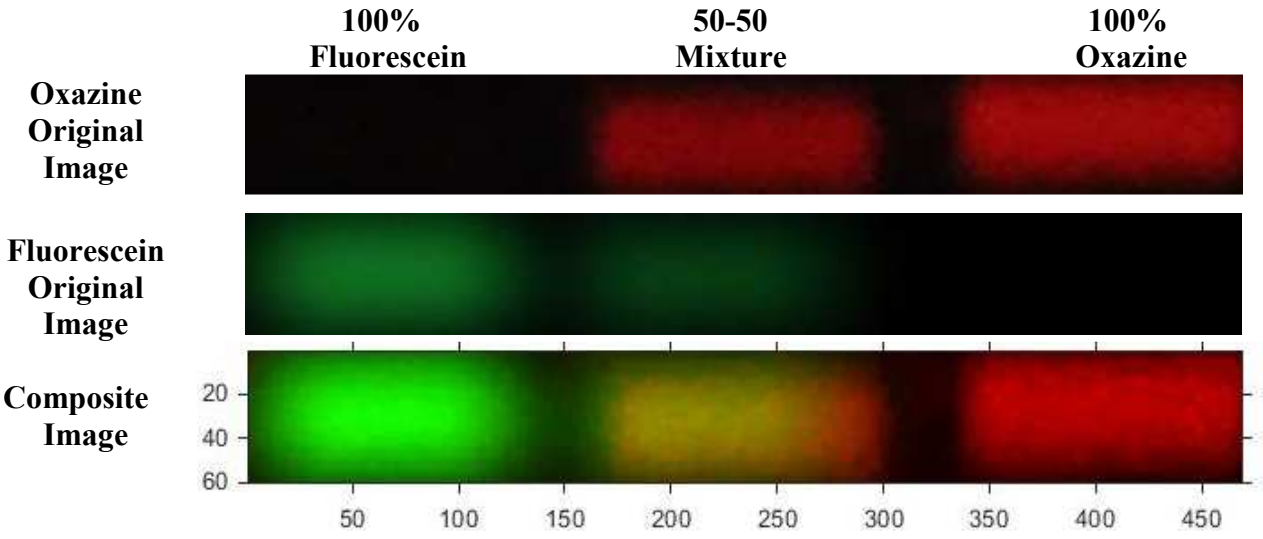

Figure 42. Cuvette experiment Matlab images

Take note that the 100% oxazine solution is not visible in the original fluorescein image and the 100% fluorescein solution is not visible in the original oxazine image, depicting the ability of the DPLIF system to be able to only detect the intended fluoresced species in its designated camera. Also, the composite image displays a yellow color for the 50-50 mixture (middle) cuvette, signifying similar intensity between fluorescein and oxazine, further depicting the DPLIF system's ability to detect the interaction of the liquid mixtures accurately. To better

quantify this performance, Figure 43 presents a line profile analysis of the 50-50 mixture, using ImageJ software. The line profile indicated that the 50-50 mixture did not produce a 50% reduction in intensity from the 100% solutions for both oxazine and fluorescein. Both the fluorescein and oxazine intensity values were greater than that of half the 100% solution intensity by 10 and 15 gray scale values, respectively. Therefore, calibration curves for both oxazine and fluorescein solutions were performed. The results are displayed in Figure 44.

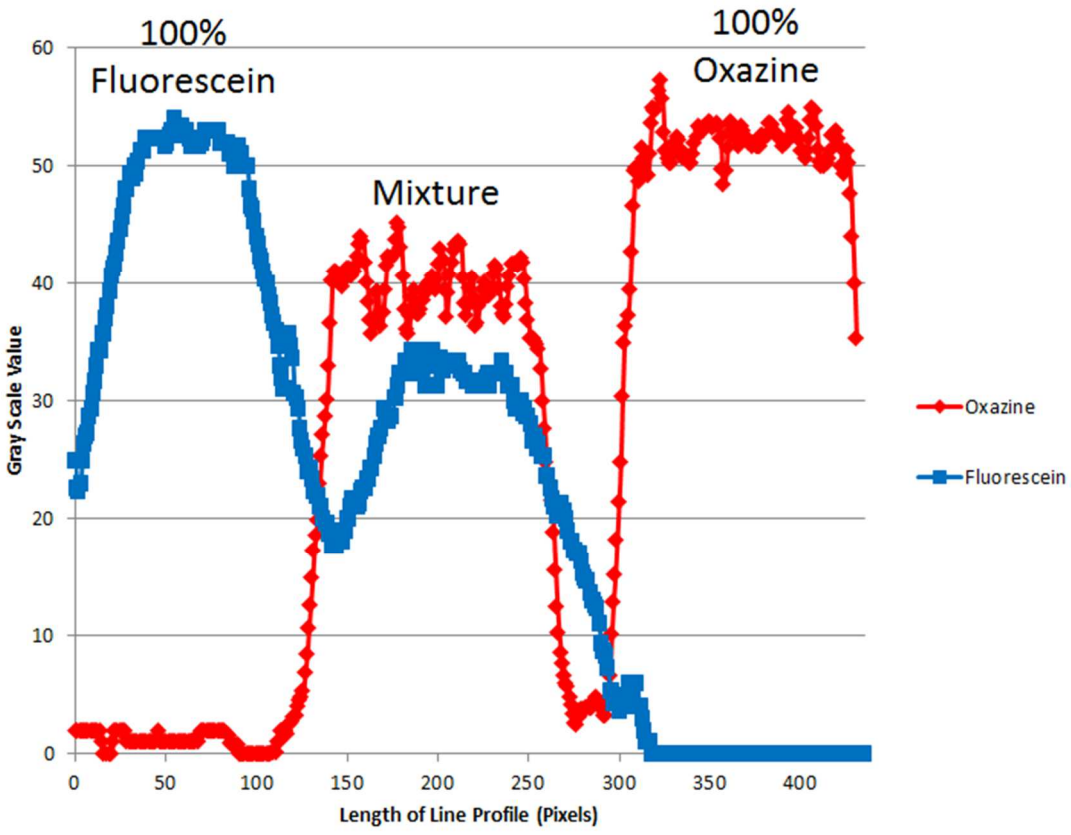

Figure 43. Line profiles of original oxazine and fluorescein cuvette test images

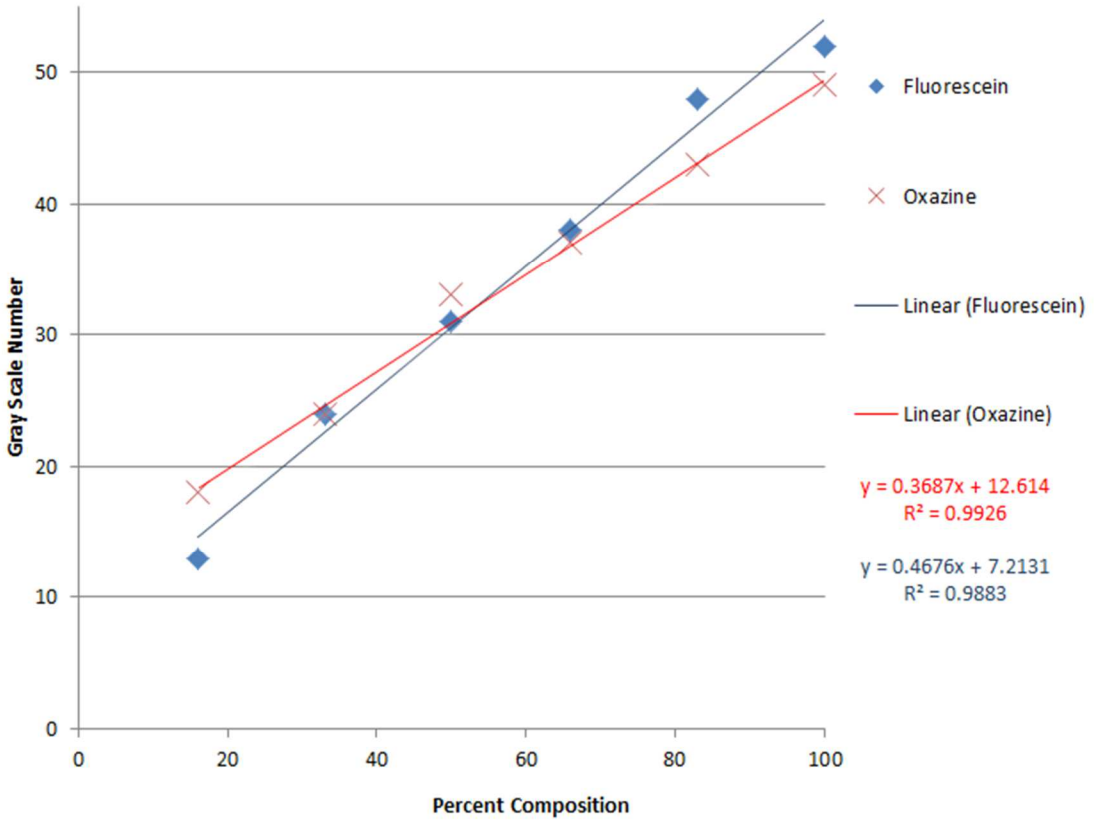

Figure 44. Fluorescent intensity calibration curves for cuvette experiments

The results indicate a linear relationship between the concentration of oxazine and fluorescein present in the solution and the intensity of the fluorescence of each. The offset in the mixture results could be due to spectral response overlap of the red, green and blue (RGB) channels in the Nikon D90 color sensor. Figure 45 displays the RGB spectral response curves from a Nikon D90 with and without a BG55 filter (Llado Gambin et al., 2015). The purple sections displayed in the figure depict the wavelength range of the bandpass filters used in the DPLIF system. Take note that the "tails" of the red, green and blue spectral response filter curves overlap within the bandpass filter ranges. Also, take note that red has a higher relative intensity in the fluorescein (green) detection region than green has in the oxazine (red) detection region. The trends presented in Figure 45 support the data presented in Figure 43, where the oxazine signal is larger than the fluorescein signal in the 50-50 mixture. Therefore, overlap of the spectral

response curves in the Nikon D90 camera may contribute to the increased fluorescence signal in the mixture compared to the pure samples. Alternatively, the fluorescence intensity offset could be due to instrumental noise. The results obtained from the calibration curves will be implemented into future image analysis to mitigate potential errors present that are responsible for the discrepancies between the experimental and predicted values.

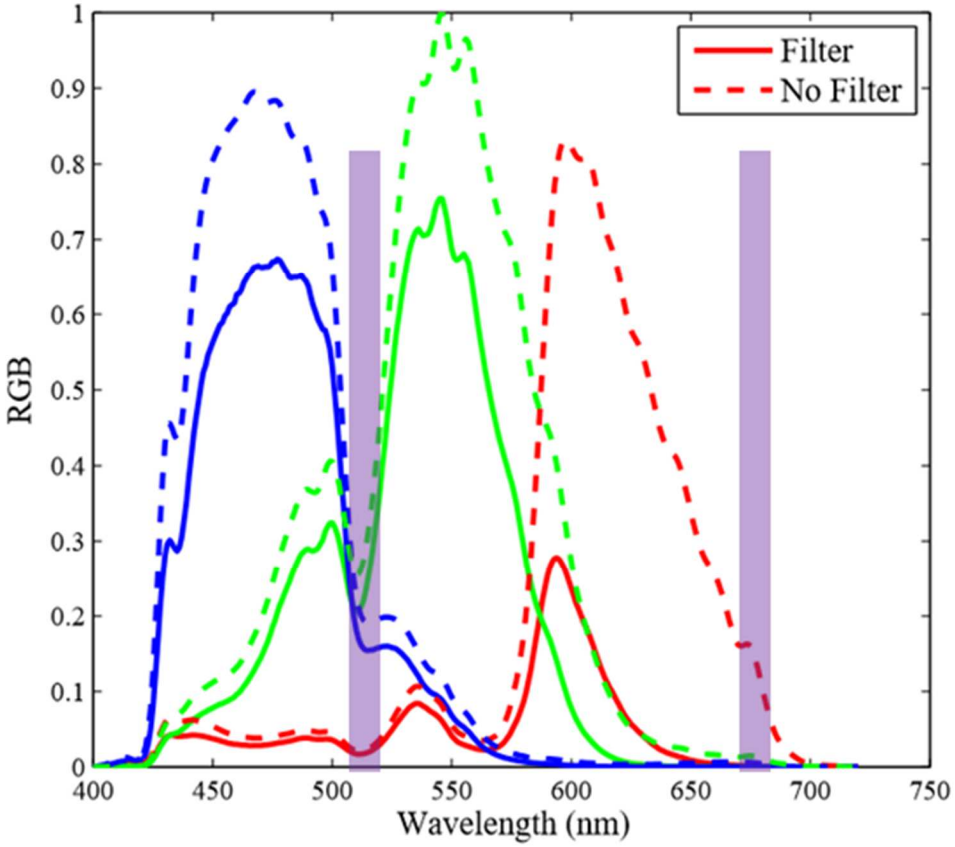

Figure 45. RGB spectral response curves in a Nikon D90 camera with and without a BG55 filter (Llado Gambin et al., 2015) and bandpass filter ranges (purple) used throughout the DPLIF experiments

4.3.2 Spray Experiments

To further test the functionality and reliability of the DPLIF system, spray experiments were performed. Fluorescent mixing data was collected from the DPLIF system and analyzed for both a simplex nozzle injector and unlike doublet injectors.

Simplex Nozzle Injector

Spray experiments were performed using a full cone pressure swirl simplex nozzle, as displayed in Figure 46 (Rimbert, N., 2010). The experimental setup for the simplex nozzle experiments is similar to the setup displayed in the Instrument Integration section. However, where the unlike doublet injectors are displayed in the CAD design, a simplex nozzle is present. The oxidizer and fuel flows come into the nozzle from their respective tanks via a T-Swagelok fitting. Through this setup, it is possible to only flow oxazine solution, fluorescein solution or a mixture at various mass flow rates.

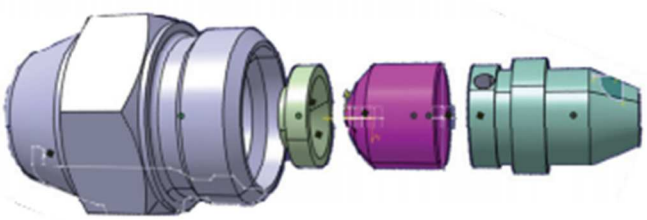

Figure 46. Full cone pressure swirl simplex nozzle (Rimbert, N., 2010).

In the simplex nozzle spray experiments, the nozzle centerline was placed onto the rig at a 90° angle in relation to the planar laser sheet. In order to analyze the mixing of the two injector streams, one expelling a 20μM oxazine solution and the other a 20μM fluorescein solution, the system needed to be "blanked". Therefore, optimal parameters (laser current (power), camera ISO and camera exposure time) for this test were determined where the fluorescent intensities of each pure fluorescein and pure oxazine spray equaled each other. Furthermore, the mass flow rate of the spray was kept constant at 12lb/hr for both fluorescent solutions during the "blanking"

experiments. The optimal parameters used in the simplex nozzle injector experiments are displayed below in Table 8 and a schematic of the experimental setup is displayed in Figure 47.

Table 8. Optimal parameter settings for simplex nozzle injector experiments

Fluorescent of Interest	Laser Current (Amps)	Camera ISO	Camera Exposure Time (seconds)
Oxazine	2.12	3200	15
Fluorescein	1.23	2000	15

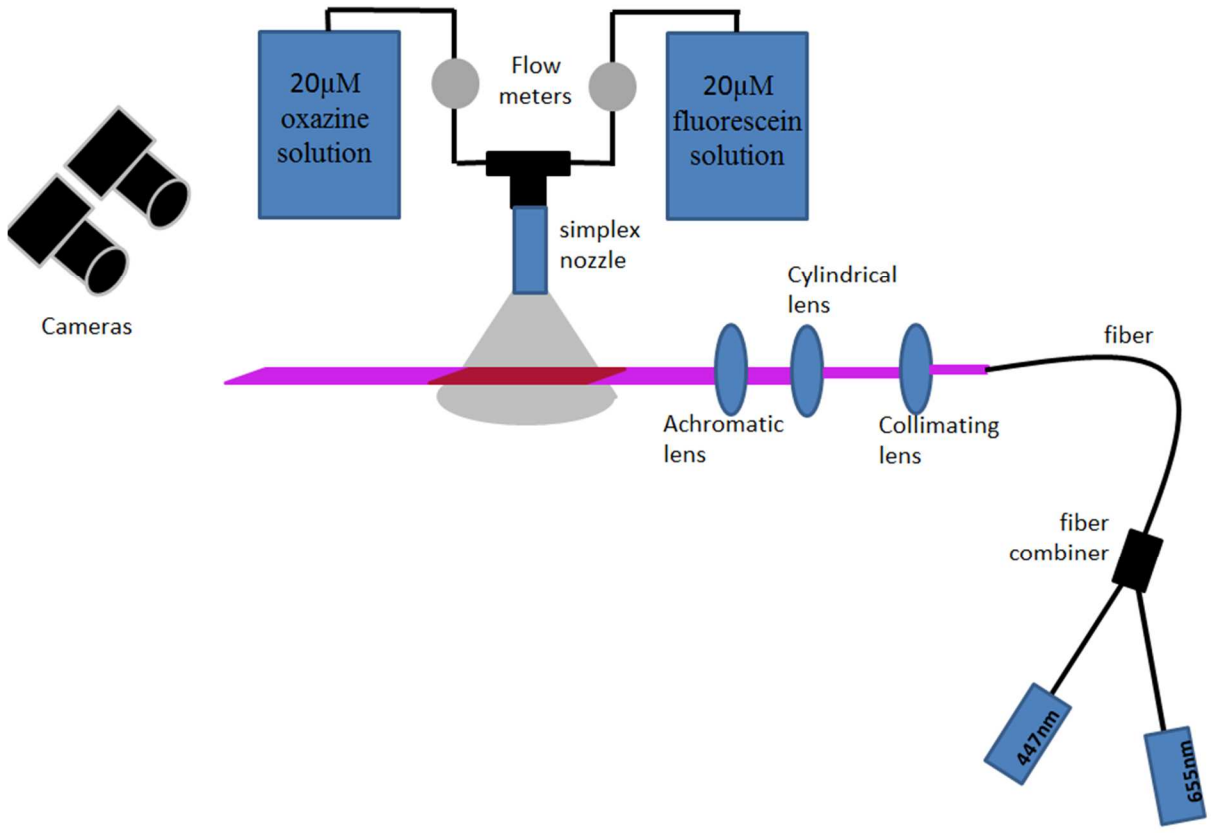

Figure 47. Simplex nozzle spray experimental setup

Once the system had been "blanked" a 50-50 mixture was tested at a total mass flow rate of 24lb/hr, with the mass flow rate of both solutions set to 12lb/hr, respectively. Next, a series of 6 cuvettes were placed under the spray where the liquid was collected. The cuvette experimental setup is displayed below in Figure 48. The planar laser sheet then illuminated the spray collected in the cuvettes and the fluorescence was captured by the cameras. The images collected from the DPLIF camera system were then analyzed using the optimized Matlab code. The spray images and cuvette images are displayed below in Figure 49.

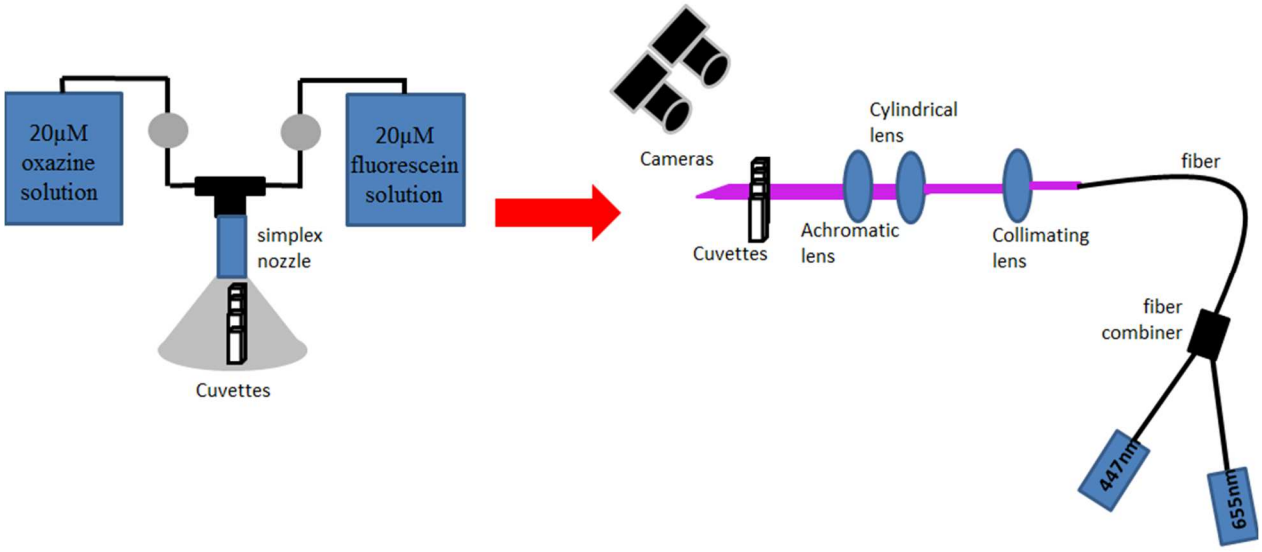

Figure 48. Simplex nozzle cuvette experimental setup

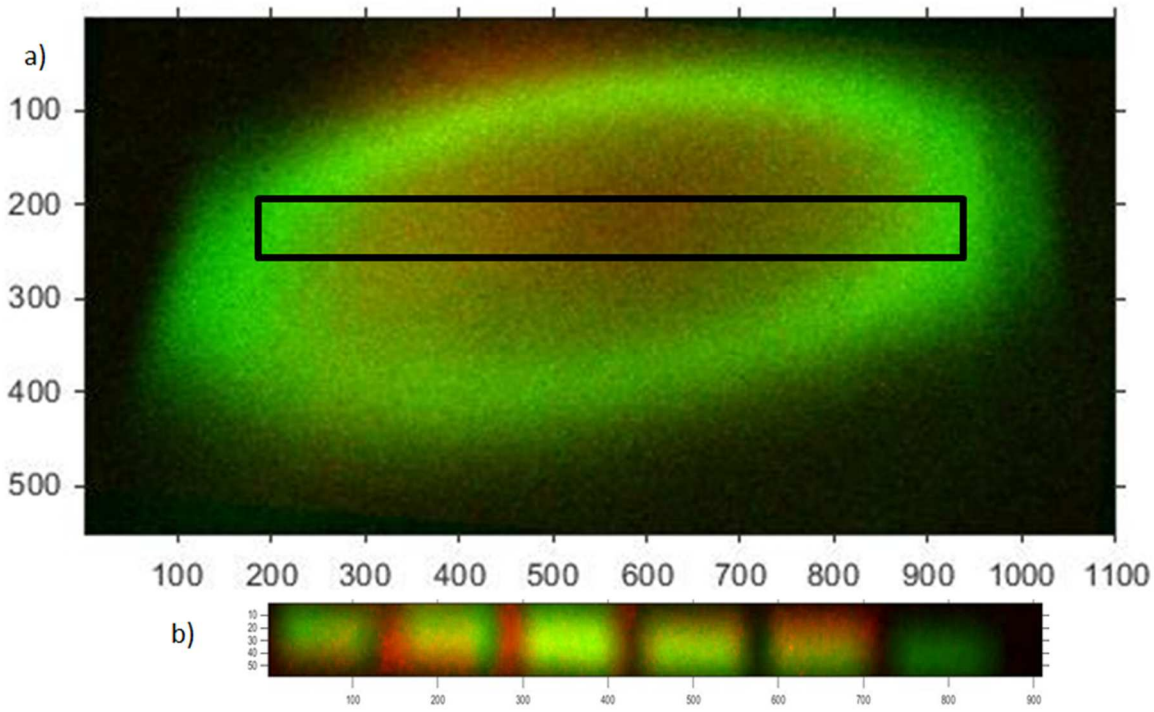

Figure 49. Simplex nozzle experiment Matlab images: a) Simplex nozzle spray Matlab composite image b) Simplex nozzle spray collected cuvette Matlab composite image

Take note that the black box in the spray composite image indicates the area of the spray collected by the cuvettes. It is apparent in the spray image that fluorescein liquid is dominant on the outside of the spray and makes a ring shape. The middle of the spray depicts a mixture of the fluorescein and oxazine, represented by the lighter green, yellow, and red pixels. The spray collected in the cuvettes displays a similar pattern as to that presented in the spray images. For example the outer cuvettes depict fluorescein as the more dominant liquid, where the inner four cuvettes display a mixture of oxazine solution and fluorescein solution as depicted by the yellow, green and red colored pixels in the composite cuvette image. It was expected that the simplex nozzle should produce a homogenous mixture throughout the spray. However, that is not the mixing pattern seen in the DPLIF results. The spray structure seen in the DPLIF results could be due to mixing inefficiencies when the fluorescein and oxazine solutions combine via a T-

Swagelok at the back end of the nozzle. Further steps will need to be taken in the future, to mitigate the mixing inconsistency, however the experimental spray structure does not take away from the validity of the DPLIF ability to characterize spray structure. The objective of this test was not to assess spray structure, but to compare the spray mixing with the mixing noted from the liquid collected in the cuvettes.

A quantitative analysis of the spray and cuvette images was performed in correspondence with the qualitative analysis. Line intensity profiles were taken of both the original cuvette images and the original spray images for each fluorescent solution. A comparison of the line profiles of the cuvettes compared to the spray are displayed below in Figure 50 for oxazine and in Figure 51 for fluorescein.

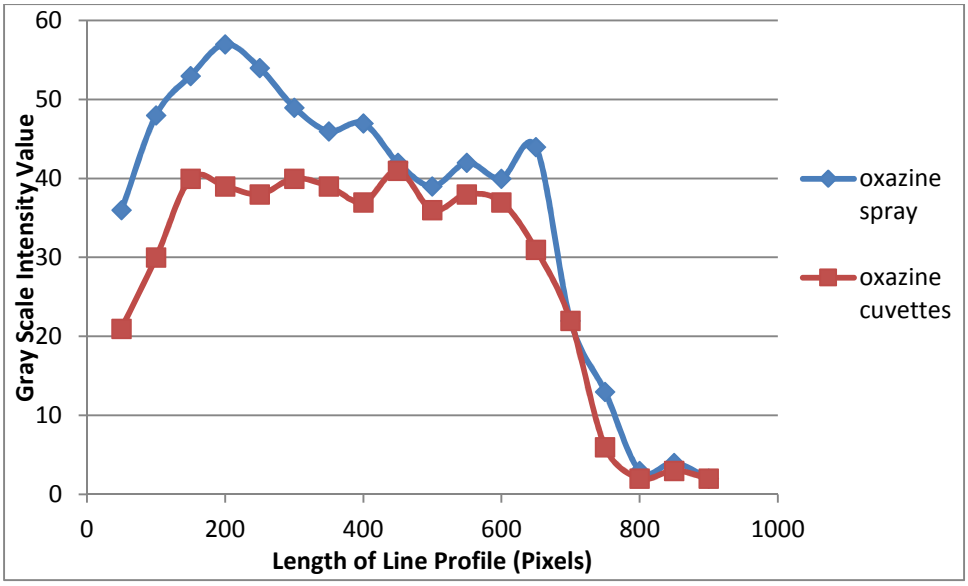

Figure 50. Oxazine solution spray and cuvettes line intensity profiles

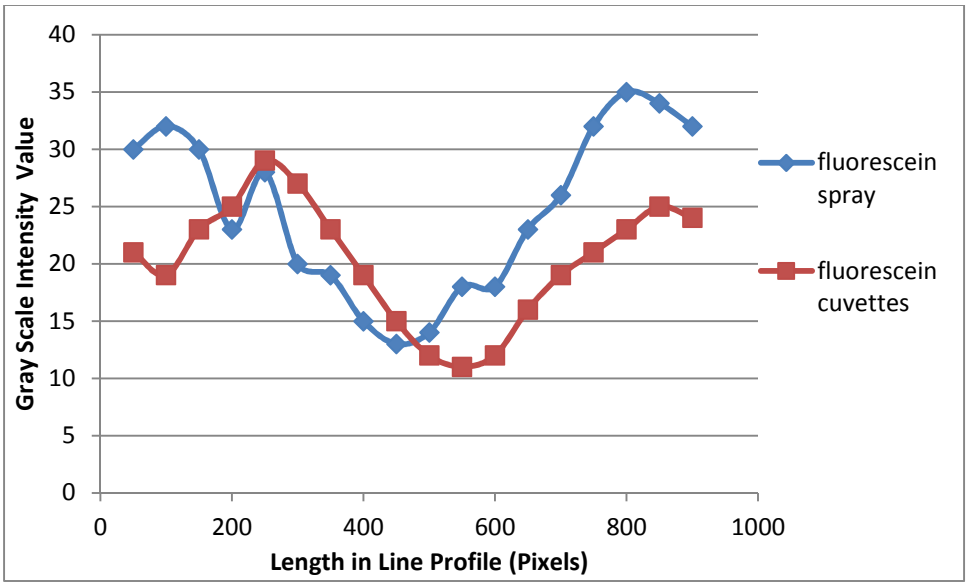

Figure 51. Fluorescein spray and cuvettes line intensity profiles

The line profiles for both the oxazine spray and cuvettes displayed in Figure 50 show similar trends. Although the line intensity profiles are not exact matches, experimental error, such as secondary splatter off of the cuvettes, could explain the discrepancies between the two line profiles. The same is true for the line profiles of the fluorescein spray and cuvettes.

The presence of the illuminated oxazine and fluorescein fluorescence in the spray images support the hypothesis that the proposed optimized DPLIF system can be used to study the liquid-liquid interactions of injector sprays. Furthermore, the spray and cuvette results support the hypothesis that the DPLIF system can accurately assess the liquid interactions with in the spray. Therefore, the qualitative analysis of the composite spray image and the composite cuvette image in conjunction with the quantitative analysis of the original spray and cuvette images, further demonstrate the functionality and accuracy of the optimized DPLIF instrumentation.

Unlike Doublet Injectors

Spray experiments were also performed on the unlike doublet injectors. The experimental setup for the unlike doublet injectors experiments was similar to that of the simplex nozzle injector and is displayed in Figure 52. The two unlike doublet injectors were set to 90° degrees apart from each other and at a 45° angle offset from the DPLIF laser sheet. Furthermore, the impingement point from the injector streams were 1cm from each nozzle and the spray was analyzed 8cm below the impingement point. Both injector streams were kept at a consistent mass flow rate of 12lb/hr.

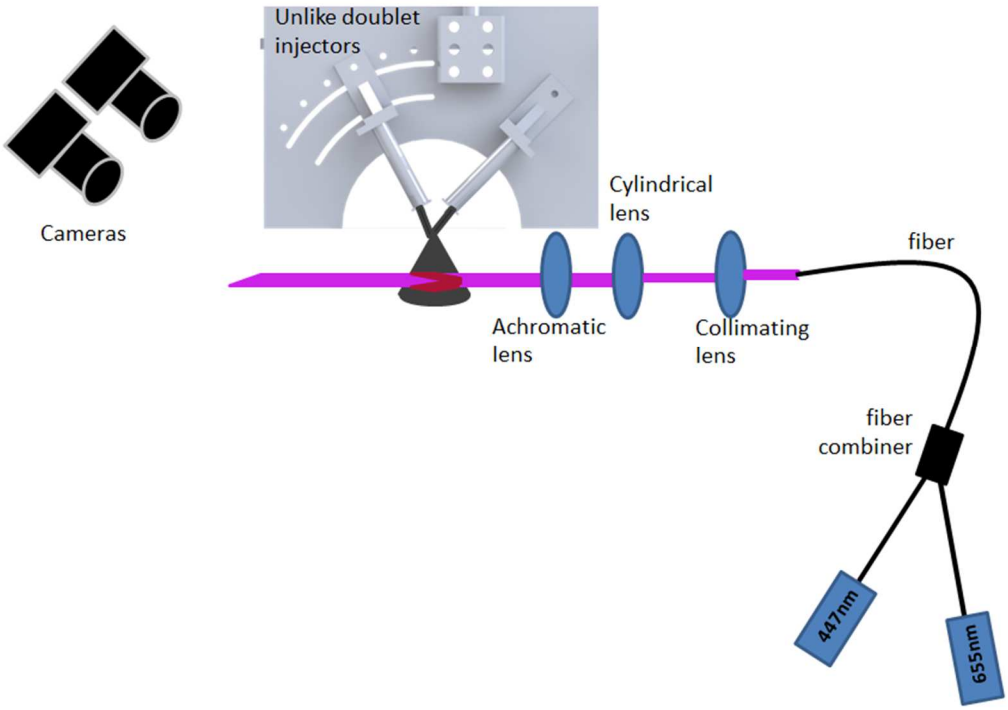

Figure 52. Unlike doublet injectors tests experimental setup

In order to analyze the mixing of the two injector streams, one expelling a 20µM oxazine solution and the other a 20µM fluorescein solution, the system needed to be "blanked". Therefore, optimal parameters (laser current (power), camera ISO and camera exposure time) for

this test were determined where the fluorescent intensities of each stream equaled that of the other. The optimal parameters used in the unlike doublet injectors experiments are displayed below in Table 9.

Table 9. Optimal parameter settings for unlike doublet injector experiments

Fluorescent of Interest	Laser Current (Amps)	Camera ISO	Camera Exposure Time (seconds)
Oxazine	2.11	Hi0.7	15
Fluorescein	0.26	1000	15

Once the system had been "blanked" the 50-50 mixture was analyzed using the optimized Matlab code. The resulting Matlab produced composite image of the two unlike doublet injectors sprays is displayed below in Figure 53. Figure 10 and Figure 54 display cartoon models of the spray portrayed in Figure 53 to aid in the visualization of the collected data.

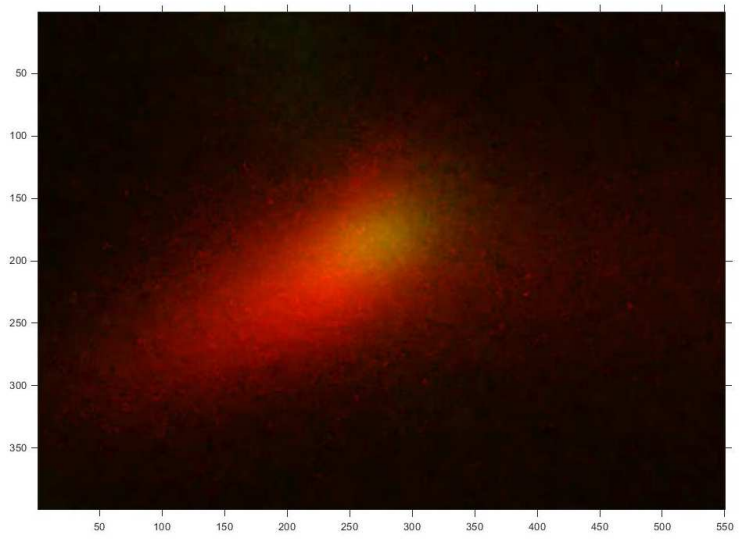

Figure 53. Matlab composite image for unlike doublet injectors experiments

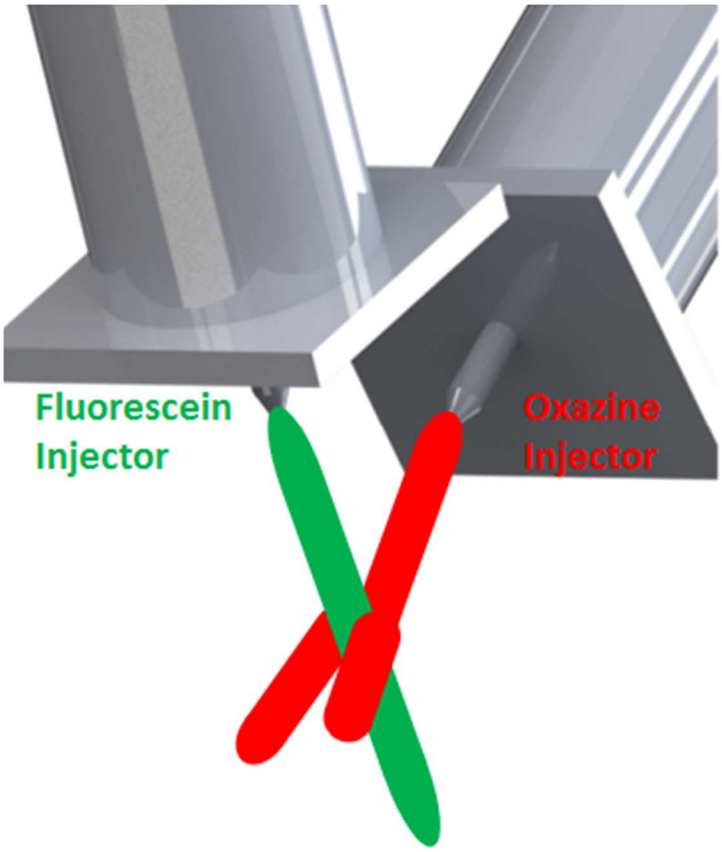

Figure 54. Doublet injector experiment composite image model

The composite image displays a predominant oxazine "tail" on the left and a region of similar intensity between oxazine and fluorescein representing the impingement point of the two jets, displayed as a yellow circle in the middle of the image. The composite image gives the impression that the fluorescein jet splits the oxazine jet, where oxazine spray is dispersed radially from the impingement point. The fluorescein injector orifice is smaller than that of oxazine, resulting in a higher velocity of fluid in the jet, despite the same initial mass flow rate. When comparing the exit velocities of each injector, the oxazine/fluorescein momentum ratio equaled 0.52. Based on studies performed by Won et al., the mixing efficiency, to describe the degree of mixing (percent) in the impinging injectors, was determined to be close to 50% for a momentum ratio of 0.5 and injector diameters of 0.4mm and 0.6mm (Won et al., 2002). The unlike doublet

injectors used in this thesis had diameters of 0.5842mm and 0.4267mm. Furthermore, studies performed by Rupe concluded that maximum mixing efficiency occurs in the region where the ratio of the areas of the fluorescein and oxazine nozzles is 0.7 (Ashgriz et al., 1995). However, in the studies performed in this thesis, the area ratio of the nozzles is 0.523, differing from what Ashgriz describes as the optimal ratio. Therefore, it is expected that the impinging doublet injector sprays would have low mixing efficiency, meaning low homogeny throughout the spray, which is congruent with the composite matlab image. Further testing will need to conducted to further understand the unlike doublet injectors spray mixing. However, the composite image presented above in Figure 53, further demonstrates the DPLIF system's ability to assess the mixing of dynamic liquid-liquid interactions.

5 SUMMARY, CONCLUSIONS, AND RECOMMENDATIONS

5.1 Summary of Results

In this effort, the proposed DPLIF system has demonstrated sufficient functionality and accuracy when assessing liquid-liquid interactions in both standing fluids and dynamic sprays. In summary:

- Nikon D90 cameras were successfully able to capture the fluorescence of oxazine and fluorescein enriched fluids.
- The chosen oxazine and fluorescein derivatives have demonstrated high quantum yield and could be detected using the optimized DPLIF system.
- Successful implementation of fiber optics into the optics system was conducted.
- A condensed Matlab program was successfully created and implemented for DPLIF data analysis.
- Cuvette experiments were performed using the DPLIF system to analyze liquid-liquid interactions in stationary fluids. The results indicated that the 50-50 mixture of fluorescein and oxazine solutions displayed similar fluorescent intensities.
- Spray experiments using a simplex nozzle injector and unlike doublet injectors were performed using the DPLIF system to analyze liquid-liquid interactions in dynamic fluids. The results indicated that the line intensity profiles of the spray collected in cuvettes and the spray images had similar trends for both fluorescents tested.

5.2 Conclusions

From the results listed above, these main conclusions can be made:

- **The optimization of the DPLIF system has led to enhanced capability.**

The DPLIF system has been enhanced through the inclusion of fiber optics to combine the two lasers into a planar sheet, use of suitable fluorescent tracers and the use of two cameras to capture the fluorescence of oxazine and fluorescein solutions at the same time. The implementation of these components enhances the operation of the DPLIF system, but also makes it more compact. The more compact, enhanced DPLIF system allows for a more commercialized system to study liquid-liquid interactions.

- **Further, the optimization reduces the total cost of the DPLIF system.**

The total cost of the DPLIF system is reduced drastically through the use of two commercial Nikon CCD D90 cameras. In previous experiments performed with the DPLIF system, an ICCD Andor camera was used. The implementation of readily available, consumer cameras reduces the price of the DPLIF camera system by as much as $40,000. The cost-effective enhancements allow the DPLIF technique to be a more feasible and desirable technique when studying the mixing characteristics of liquid-liquid interactions, especially sprays.

- **The preliminary results indicate high functionality and accuracy of the DPLIF system.**

The cuvette experiments along with the spray experiments give promising preliminary results. The results obtained from these experiments support the hypotheses that the proposed optimized DPLIF system can efficiently and accurately assess the liquid-liquid interactions of stationary fluids along with highly dynamic sprays. The ability of the DPLIF system to provide accurate assessments of liquid-liquid interactions of stationary fluids and dynamic sprays provides a robust, novel technique to help assess and ultimately predict functionality of liquid systems, such as spray injectors.

- **The DPLIF system can ultimately be used to better understand and characterize rocket injector sprays.**

After further proof of concept testing, the DPLIF system can be used to analyze and understand rocket injector sprays, to ultimately design and manufacture more enhanced rocket injectors. Currently, rocket injector performance is assessed using expensive, time-consuming hot-fire tests. Through the use of the less expensive, accurate DPLIF technique, it is possible to further understand the mixing of oxidizer and fuel within rocket injector sprays and predict performance through a more cost-effective, time-efficient approach.

- **The enhanced DPLIF system is a viable technique to better understand liquid-liquid interactions in standing fluids and dynamic sprays.**

The results from the cuvette tests along with the results from the spray tests display suitable accuracy and functionality of the instrument to assess standing liquids as well as dynamic sprays. The enhanced DPLIF instrumentation utilizes a low cost, compact dual laser-camera system to assess the liquid interactions of two fluids (fuel and oxidizer) through the fluorescence of two liquids, which is commercially appealing. Therefore, the DPLIF technique is a new, viable method for understanding mixing interactions, ultimately allowing for a more feasible, cost-effective way to study rocket injector sprays for design enhancement.

5.3 Recommendations

To improve upon this research and further optimize the system, here are a few recommended tasks that can be performed.

- The DPLIF system can be further optimized in order to make it more cost effective and reliable. For instance, the optics system can be further condensed through the use of

different lenses and/or optical techniques. The cost of the camera system can be lowered further through the potential use of low-cost webcams in replacement of the Nikon D90 cameras.

- The Matlab analysis program can be further edited and reworked to have a better understanding of the underlying code that makes up the image analysis functions used. The Matlab program can also be enhanced to provide quantitative image analysis in addition to qualitative analysis.
- Calibration tests of each DPLIF system component should be performed to better understand potential errors in the system and to increase the reliability and performance of the instrument.
- The overlapping spectral response curves hypothesis for the increase in fluorescence intensity (offset) in the mixtures should be looked into further through further investigation of the theory and additional experiments.
- The hypothesis for inefficient mixing in the simplex nozzle experiments needs to be further analyzed and additional experiments should be performed to acquire the predicted homogenous mixing within the spray. For instance, perhaps moving the T-Swagelok further back from the simplex nozzle would provide adequate time and space for the two solutions to fully mix before the liquids exit the nozzle orifice.
- Different sample systems should be analyzed with the DPLIF, such as single drop analysis, in order to further test the functionality, accuracy and precision of the DPLIF system.
- DPLIF instrumentation should be used to analyze the spray characteristics of rocket injector sprays in order to enhance research in this area.

6 REFERENCES

Ashriz, N., Brocklehurst, W. and Talley, D. (1995). On the Mixing Mechanisms in a Pair of Impinging Jets, *31st AIAA/ASME Joint Propulsion Conference and Exhibit*, AIAA 95-2421, San Diego, California.

Ashriz, N., Brocklehurst, W. and Talley, D. (2001). Mixing Mechanisms in a Pair of Impinging Jets, *Journal of Propulsion and Power*, 17,3, 336-349.

Austin, B.L., Heister, S.D and Anderson, W.E. (2005)., Characterization of Pintle Engine Performance for Nontoxic Hypergolic Bipropellants, *Journal of Propulsion and Power,* 21, 4, 627-635

Bolszo, C. D. (2011). *Pressure Atomization of Water-in-Oil Emulsions and Effects of Gaseous Crossflow*, University of California, Irvine.

Brezani, I., Zelenak, F.**,** *Improving the effectivity of work with Rosin-Rammler diagram by using MATLAB® GUI tool*, Acta Montanistica Slovaca, Vol. 15, (2010).

Bruchhausen, M., Guillard F., Lemoine, F. (2005). Instantaneous measurement of two-dimensional temperature distributions by means of two-color planar laser induced fluorescence (PLIF). *Experimental Fluids* 38:123–131.

Color Versus Black and White Cameras (n.d.). In *Fluid Imaging Technologies*. Retrieved April 28, 2016, from http://info.fluidimaging.com/hs-fs/hub/300163/file-2221588320-pdf/documents/Tech_Briefs/FCTB3_BW-vs-Color_Cameras.pdf?t=1459881952118

Crimaldi, J.P., Koseff J.R. (2001). High-resolution measurements of the spatial and temporal scalar structure of a turbulent plume. *Experimental Fluids* 31(1):90–102.

Crimaldi, J.P., (2008). Planar laser induced fluorescence in aqueous flows. *Experiments in Fluids* 44(5):651-863.

D90 Specifications (n.d.). In *Nikon*. Retrieved April 22, 2016, from http://imaging.nikon.com/lineup/dslr/d90/spec.htm

Dahm, W.J.A., Dimotakis, P.E. (1987). Measurements of entrainment and mixing in turbulent jets. *AIAA Journal* 25(9):1216–1223

Dewey, C. (1976) Qualitative and quantitative flow field visualization utilizing laser-induced fluorescence. *Proceedings of the AGARD conference of non-intrusive instrumentation in fluid flow research,* AGARD-CP-193.

Digital Camera Sensors (n.d.). In *Cambridge in Colour*. Retrieved April 28, 2016, from http://www.cambridgeincolour.com/tutorials/camera-sensors.htm

Dong, Q. et al., (2013). A study on the spray characteristics of a piezo pintle-type injector for DI gasoline engines, *Journal of Mechanical Science and Technology,* 27,7, 1981-1993.

Drallmeier, J.A. (1994). Hydrocarbon vapor measurements in fuel sprays: a simplification of the infrared extinction technique, *Journal of Applied Optics,*33,30, 7175-7179.

Dressler, G.A., and Bauer, M.A. (2000). TRW Pintle Engine Heritage and Performance Characteristics, *AIAA 2000-3871, 36th AIAA/ASME/SAE/ASEE Joint Propulsion Conference and Exhibit*, Huntsville, Alabama.

Eckbreth, A.C. (1996). Laser Diagnostics for Combustion Temperature and Species, *Overseas Publishers Association*, Amsterdam, Netherlands,1-10.

Fang, X., et al. (2016) .A handheld laser-induced fluorescence detector for multiple applications. *Talanta* 150:135-141.

Fansler, T.D., Parish, S.E., (2015). Spray measurement technology: a review, *Measurement Science Technology,* 26.

Hefner, R.J. (1996). Review of Combustion Stability Development with Storable Propellants, *Journal of Spacecraft and Rockets*, 3,7, 1046-1051.

Heister, S.D. *Handbook of Atomization and Sprays: Pintle Injectors,* Springer, 647-656 (2011).

Ito, Yang, V., Habiballah, M., Hulka, J. and Popp, M. (2004). Liquid Rocket Thrust Chambers: Aspects of Modeling, Analysis, and Design, *American Institute of Aeronautics and Astronautics, inc*, 15.

Jung, K., Yoon, Y., Hwang, S., (2000). Spray Characteristics of Impinging Jet Injectors Using Imaging Techniques, *26th AIAA Joint Propulsion Conferennce and Exhibit,*AIAA-2000-3396, Huntsville, Alabama.

Kennny, R.J. et al., (2006). Cold Flow Testing for Liquid Propellant Rocket Injector Scaling and Throttling, *42nd AIAA/ASME Joint Propulsion conference,* AIAA 2006-47-5.

Kokhanovsky, A.A., *Light Scattering Reviews 10*, Springer, 252 (2016).

Komori, S., Nagata, K., Kanzaki, T., Murakami, Y. (1993). Measurements of mass flux in a turbulent liquid flow with a chemical-reaction. *AICHE Journal* 39(10):1611–1620.

Koochesfahani, M.M., Dimotakis, P.E. (1986). Mixing and chemical reactions in a turbulent liquid-mixing layer. *Journal of Fluid Mechanics* 170:83–112

Kuo, K.K. *Recent Advances in Spray Combustion: Spray Combustion Measurements and Model Simulation Volume II,* American Institute of Aeronautics and Astronautics, 178 (1996).

Kychakoff, G., Howe, R.D., Hanson, R.K. andMcDaniel, J.C. (1982). Quantitative visualization of combustion species in a plane, *Applied Optics* 21, 3225-3227.

Lai, W.H. and. Wang, H.C., (2002). Flow Patterns Generated by Like and Unlike Doublet Impinging Jets, *38th AIAA/ASME Joint Propulsion Conference and Exhibit ,* AIAA 2002-3700, Indianapolis, Indiana.

Le Gal, P., Farrugia, N. and Greenhalgh, D.A. (1999). Laser Sheet Dropsizing of dense sprays, *Optics and Laser Technology* 31, 75-83.

Lefebvre, A.W., *Gas Turbine Combustion*, McGraw-Hill, 204 (1999).

Llado Gambin, A., Padilla, R.E., Dunn-Rankin, D., and Pham, T. K., (2015). Color-ratio pyrometry for temperature measurements in methane/air counterflow flames, *9th U.S. National Combustion Meeting*, Paper#:114LF-0323, Cincinati, Ohio.

Herman, B. et al. (2012), Basic Concepts in Fluorescence, In *Microscopy Resource Center*, Retrieved March 18, 2016, from http://www.olympusmicro.com/primer/techniques/fluorescence/fluorescenceintro.html

Lockett, R., et al. (2016). An optical characterization of atomization in non-evaporating diesel sprays. *SAE International*, 2016-01-0865.

Maetzler, C. (2002). MATLAB Functions for Scattering Absorption. *Institut für Angewandte Physik*, Research Report No. 2003-08, 4.

Mathworks: Imfuse Composite Image (2012). In *Mathworks.* Retrieved October 18, 2015, from http://www.mathworks.com/help/images/ref/imfuse.html#inputarg_method

McDonell, V. and Samuelsen, S. (1997). Assessment of liquid fuel distribution in sprays using planar imaging methods. *Asia-Pacific Conference on Combustion*, Osaka, Japan.

McDonell, V., Phi, V., Samuelsen, S. (1999). Structure of sprays generated by unlike doublet injectors. *American Institute of Aeronautics and Astronautics*.

Melton L.A., (1993). Exciplex-based vapor/liquid visualization systems appropriate for automotive gasolines *Appl. Spectrosc*. 47, 782–6

Mueller, T. and Dressler, G. (2000). TRW 40 KLBf LOX/RP-1 Low Cost Pintle Engine Test Results, *AIAA 2000-3863*, *36th AIAA/ASME/SAE/ASEE Joint Propulsion Conference and Exhibit*, Huntsville, Alabama.

Oxazine725 (n.d.) In *Fluorophores.* Retrieved January 12, 2016, from www.Fluorophores.org

Oxazine750 (n.d.) In *Fluorophores.* Retrieved January 12, 2016, from www.Fluorophores.org

Papantoniou, D., List, E.J. (1989). Large-scale structure in the far field of buoyant jets. *Journa l of Fluid* Mechanics 209:151–190.

Prasad, R.R., Sreenivasan, K.R. (1990). Quantitative 3-dimensional imaging and the structure of passive scalar fields in fully turbulent flows. *Journal of Fluid Mechanics* 216, 1–34.

Purdue University AEE539: Liquid Rocket Engine Injectors. (2007).

Rauwendaal, C. *Mixing in Polymer Processing.* Marcel Dekker, Inc., 1-2. (1991).

Reynolds, O. (1883). An experimental investigation of the circumstances which determine whether the motion of water in parallel channels shall be direct or sinuous and of the law of resistance in parallel channels. *Philosophical Transactions of the Royal Society* 174:935–982.

Rimbert, N., Castanet, G., (2010). Liquid Atomization out of a Full Cone Pressure Swirl Nozzle. *Cornell University Library*.

Ryan, H.M., Anderson, W.E., Pal, S. and Santoro, R.J. (1995). Atomization Characteristics of Impinging Liquid Jets, *Journal of Propulsion and Power*, 11,1, 135-145.

Salgues, D. et al., (2006). Shear and Swirl Coaxial Injector Studies of LOX/GCH4 Rocket Combustion Using Non-Intrusive Laser Diagnostics, *44th AIAA Aerospace Sciences Meeting and Exhibit*, AIAA 2006-757, Reno, Nevada.

Shock, E.L., Schulte, M.D., (1998). Organic synthesis during fluid mixing in hydrothermal systems. *Journal of Geophysical Research,* 103, E12, 28513-28527.

Skoog, D.A., Holler, E.J., Crouch, S.R., *Principles of Instrumental Analysis,* Thompson Books, 400-403 (1998).

SpaceX: Falcon 9. In *SpaceX*. Retrieved January 24, 2015, from http://www.spacex.com/falcon9

Sreenivasan, K.R., Prasad, R.R. (1989). New results on the fractal and multifractal structure of the large schmidt number passive scalars in fully turbulent flows. *Physica D* 38(1–3):322–329.

Strakey, P. A. et al., (2001). Mixing Characteristics of Coaxial Injectors at High Gas/Liquid Momentum Ratios, *Journal of Propulsion and Power*, 17,2,402-410.

Sung, M. (2014). *Influence of Stream Injection in Water-in-Oil Emulsions on Diesel Fuel Combustion Performance,* University of California, Irvine.

The iStar ICCD. In *Andor*. Retrieved February 16, 2016, from http://www.andor.com/pdfs/literature/Andor_iStar_ICCD_Brochure.pdf

Thermo Fisher Scientific: Life Technologies Fluorescence SpectraViewer. In *Thermo Fisher Scientific*. Retrieved November 19, 2015, from http://www.thermofisher.com/us/en/home/life-science/cell-analysis/labeling-chemistry/fluorescence-spectraviewer.html

Thor Labs: Longpass Dichroic Mirrors/Beamsplitters: 550nm Cutoff Wavelength (n.d.). In *Thor Labs*. Retrieved February, 2, 2016 from http://www.thorlabs.us/newgrouppage9.cfm?objectgroup_id=3313#8051

Van De Hulst, H.C., *Light Scattering By Small Particles,* Dover Publications, 31, 288 (1981).

Van Vliet, E., Van Bergen, S.M., Derksen, J.J., Portela, L.M., Van den Akker, H.E.A. (2004). Time-resolved, 3D, laser-induced fluorescence measurements of fine-structure passive scalar mixing in a tubular reactor. *Experimental Fluids* 37(1):1–21

Vingert, Gicquel, Ledou, et al., (2004). Liquid Rocket Thrust Chambers: Aspects of Modeling, Analysis, and Design, *American Institute of Aeronautics and Astronautics, inc,*106.

Won, Y.D., Cho, Y.H., Lee, S.W., Yoon, W.S., (2002). Effect of Momentum Ratio on the Mixing Performance of Unlike Split Triplet Injectors, *Journal of Propulsion and Power,* 18,4,847-854.

Wong, D. (n.d). Electronic Spectroscopy: Theory. In Chemwiki. Retrieved April 11, 2016, from http://chemwiki.ucdavis.edu/Core/Physical_Chemistry/Spectroscopy/Electronic_Spectroscopy/Electronic_Spectroscopy%3A_Theory

7 APPENDIX A: Matlab Code for Image Analysis

```
dicomwrite( imread('_DSC0200_cropped.JPG'), '_DSC0200_cropped.dcm');   %will be RED in image
A = dicomread('_DSC0200_cropped.dcm');
%A2=imresize(A,1);
RA = imref2d(size(A));
%imref2d() creates an imref2d object with default property settings

dicomwrite( imread('_DSC0177_cropped.JPG'), '_DSC0177_cropped.dcm'); %will be green in image
B= dicomread('_DSC0177_cropped.dcm');
B2=imresize(B,1); %to resize B
%B2 = imresize(A,scale) returns image B that is scale times the size of A.
%The input image A can be a grayscale, RGB, or binary image.
%If scale is from 0 through 1.0, B is smaller than A. If scale is greater than 1.0, B is larger than A. By default, imresize uses bicubic interpolation.
RB = imref2d(size(B2));
%imref2d() creates an imref2d object with default property settings

RB.XWorldLimits = RA.XWorldLimits;
RB.YWorldLimits = RA.YWorldLimits;
%Minimum and maximum coordinate values in X and Y dimension in world coordinate system, specified as a two-element numeric vector, such as [0.5 256.5].

[C,RC] = imfuse(A,RA,B2,RB,'falsecolor','Scaling','joint','ColorChannels',[1 2 0]); %Areas of similar intensity are YELLOW. if not similar intensity, are GREEN or RED based on which image
imshow(C,RC,'InitialMagnification','fit')
```